Université de Montréal

A detailed study of the lithiation of iron phosphate as well as the development of a novel synthesis of lithium iron silicate as cathode material for lithium-ion batteries

par

Karen Galoustov

Département de chimie

Faculté des arts et des sciences

Mémoire présenté à la Faculté des études supérieures

en vue de l'obtention du grade de

Maitrise (M.Sc.)

en chimie

Mars 2011

Universite de Montréal

Faculté des arts et des sciences

Ce mémoire institulé:

A detailed study of the lithiation of iron phosphate as well as the development of a novel synthesis of lithium iron silicate as cathode material for lithium-ion batteries

Présenté par

Karen Galoustov

a été évalué par le jury composé des personnes suivantes:

Président rapporteur : Pr. Garry Hanan (Université de Montréal)

Directeur de recherche : Pr. Dean MacNeil (Université de Montréal)

Membre du jury : Pr. Dominic Rochefort (Université de Montréal)

Résumé

Dans cette thèse nous démontrons le travail fait sur deux matériaux de cathodes pour les piles lithium-ion. Dans la première partie, nous avons préparé du phosphate de fer lithié ($LiFePO_4$) par deux méthodes de lithiation présentées dans la littérature qui utilisent du phosphate de fer ($FePO_4$) amorphe comme précurseur. Pour les deux méthodes, le produit obtenu à chaque étape de la synthèse a été analysé par la spectroscopie Mössbauer ainsi que par diffraction des rayons X (DRX) pour mieux comprendre le mécanisme de la réaction. Les résultats de ces analyses ont été publiés dans Journal of Power Sources.

Le deuxième matériau de cathode qui a été étudié est le silicate de fer lithié (Li_2FeSiO_4). Une nouvelle méthode de synthèse a été développée pour obtenir le silicate de fer lithié en utilisant des produits chimiques peu couteux ainsi que de l'équipement de laboratoire de base. Le matériau a été obtenu par une synthèse à l'état solide. Les performances électrochimiques ont été obtenues après une étape de broyage et un dépôt d'une couche de carbone. Un essai a été fait pour synthétiser une version substituée du silicate de fer lithié dans le but d'augmenter les performances électrochimiques de ce matériau.

Mots clés : Piles lithium-ion, matériau de cathode, amorphe, lithiation, phosphate de fer lithié, siliate de fer lithié, spectroscopie Mössbauer.

Abstract

In this thesis, we demonstrate work on two different cathode materials for lithium-ion batteries. First, the synthesis of lithium iron phosphate ($LiFePO_4$) is reproduced from literature using two lithiation methods starting with amorphous iron phosphate ($FePO_4$). For both reactions, the product at each step of the synthesis was analyzed using Mössbauer Spectroscopy and X-ray diffraction in order to gain further insight of the reaction mechanism. The results of this work were published in Journal of Power Sources.

The second cathode material of interest was lithium iron silicate (Li_2FeSiO_4). A novel synthetic method was developed to produce lithium iron silicate cost effectively starting with low cost precursors and basic laboratory equipment. The material was synthesized using a solid-state synthesis after milling and carbon coating, electrochemical performance was evaluated. An attempt was made to synthesize off-stoichiometric lithium iron silicate in order to increase the electrochemical performance of the material.

Keywords: Lithium-ion batteries, cathode materials, amorphous, lithiation, lithium iron phosphate, lithium iron silicate, Mössbauer Spectroscopy.

Table of Contents:

List of Tables:

List of Figures:

List of Abbreviations:

Ah - Ampere hour

Ci - Curie unit

d - Separation of the planes of atoms in a crystal

DSC - Differential scanning calorimetry

E_{cell} - Voltage associated with a specific electrochemical system

F - Faraday constant

ΔG - Gibbs free energy

IS - Isomer shift

LiTFSi - Lithium bistrifluoromethanesulfonamide

$LiPF_6$ - Lithium hexafluorophosphate

$LiCoO_2$ - Lithium cobalt oxide

Li-ion - Lithium ion

$LiFePO_4$ - Lithium iron phosphate

Li_2FeSiO_4 - Lithium iron silicate

$LiMn_2O_4$ - Lithium manganese oxide

$LiTiS_2$ - Lithium titanium disulfide

POE - Polyoxyethylene

QS - Quadrupole splitting

rpm - Rotation per minute

S - Siemens

TGA - Thermogravimetric analysis

V - Volt

VC - ascorbic acid

wt% - Weight percent

Wh - Watt hour

XRD - X-ray diffraction

λ - Wavelegth

Acknowledgments

First and foremost, I would like to thank my supervisor, Dr. Dean MacNeil who helped me with each step of this thesis. His work ethic and his devotion to his students encouraged me to continue to work hard and not give up when things got tough. I can safely say that I have learned a lot from him and not only about batteries.

Also, I would like to thank all the members of the MacNeil group. I enjoyed every day that I spend in the laboratory because of them. I want to thank them for the coffee break discussions that lead to interesting ideas and exciting experiments.

Finally, I would like to thank my family and my friends. Their constant support throughout this thesis kept me grounded and helped me to focus. I want to thank them for the times they listened to me talk about my research and allowed me to vent my frustration about unsuccessful experiments. Thank you all for this wonderful experience.

"Science is simply common sense at its best." ~Thomas Huxley

Karen Galoustov

Chapter 1

General Introduction

1.1 Introduction

Starting from the basics, a battery is an electrochemical cell that converts stored energy into electricity via a chemical reaction. There are two classifications for batteries: primary and secondary. In the case of primary batteries, once all the chemical energy is consumed the battery is no longer operational. Secondary batteries on the other hand, are rechargeable such that the chemical reaction is reversible.

Batteries are composed of two electrodes (anode and cathode) along with an electrolyte. The electrolyte separates both electrodes. During discharge, electrons flow from the anode to the cathode via an external circuit. The cathode is reduced and the anode is oxidized. Since the electrons flow from the anode to the cathode, the anode is at a negative potential relative to the cathode. Hence, the anode is referred to as the negative electrode and the cathode as the positive electrode [1, 2].

Rechargeable lithium-ion (Li-ion) batteries are used in various portable electronic devices as a power supply. Figure 1.1 depicts a Li-ion battery during discharge. The anode is typically composed of various types of graphite and the cathode can be composed of $LiFePO_4$, $LiMn_2O_4$, or $LiCoO_2$ among many others. The electrolyte is a lithium salt ($LiPF_6$ for example) which is

dissolved in an organic solvent. In this description, it will be assumed that the anode is composed of graphite and the cathode of $LiCoO_2$.

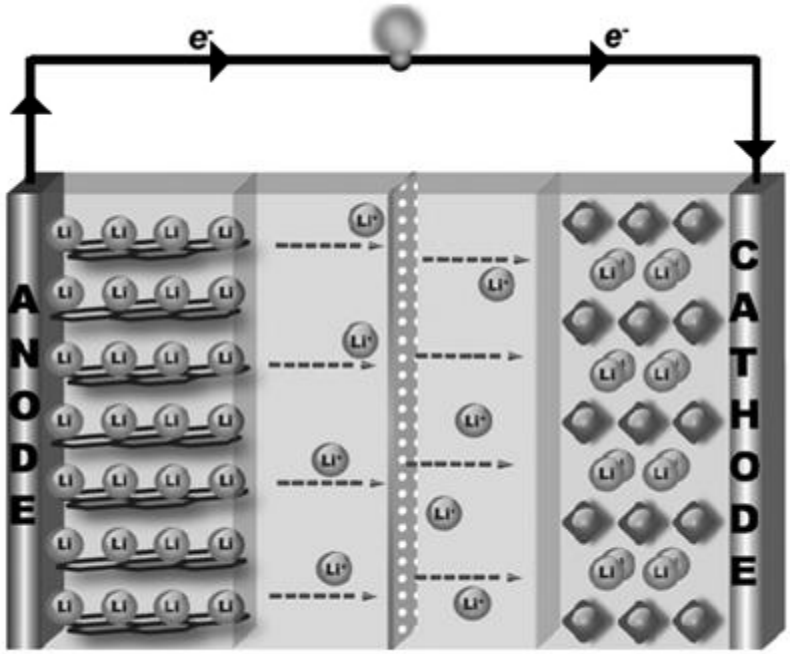

***Figure 1.1**: Schematic diagram of a discharging Li-ion battery [1]*

Upon discharge, lithium ions leave the graphite lattice and travels through the electrolyte towards the cathode. The associated electron from the lithium atom travels via an external path from which work can be performed upon placing a resistive load. The electrochemical half reaction at the anode is presented below,

$$LiC_{6(s)} \rightarrow 6C_{(s)} + Li^{+} + e^{-}. \qquad (1.1)$$

At the cathode, lithium is inserted inside the CoO_2 lattice and the electron reduces the cobalt atom from Co^{3+} to Co^{2+}. The half reaction at the cathode is presented below:

$$Li^+ + e^- + Co^{3+}O_{2(s)} \rightarrow LiCo^{2+}O_{2(s)} \quad (1.2)$$

The overall process is reversible. Upon combining equations (1.1) and (1.2), a final reaction describing the battery charging and discharging process is obtained:

$$LiC_{6(s)} + CoO_{2(s)} \underset{Discharging \rightarrow}{\overset{\leftarrow Charging}{\rightleftharpoons}} LiCoO_{2(s)} + 6C_{(s)} \quad (1.3)$$

Different battery systems are used for various applications. Each system has its specifications and its chemical characteristics. All battery systems have a common property which is to store and convert energy. In simple terms, the storage of energy is referred to how much energy can be stored in one unit of mass, specific energy (Wh kg^{-1}) or one unit of volume, energy density (Wh L^{-1}). Specific energy is the product of the capacity (mAh g^{-1}) and cell voltage (V). The capacity of a battery system is the amount of electrons exchanged during the redox reactions per gram of active material and the cell voltage is the potential difference of the redox reactions. In a plot of cell voltage versus discharge capacity (Figure 1.2), specific energy would be represented as the area under the curve [1,2].

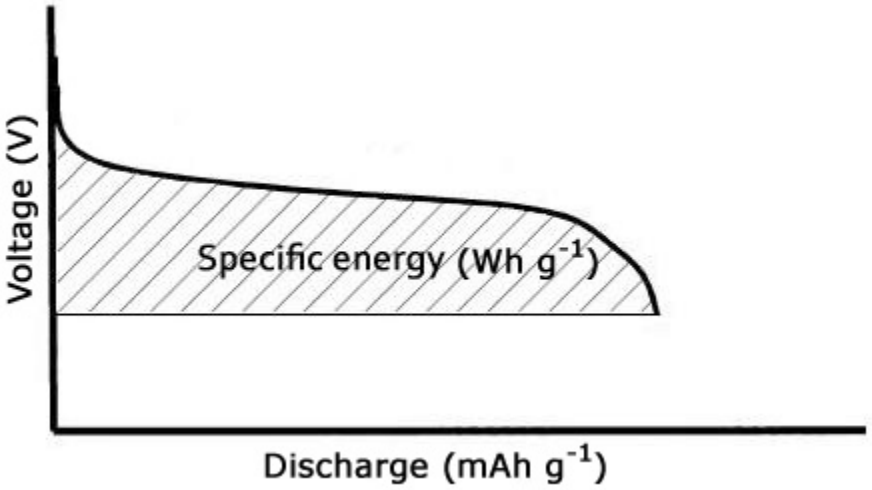

Figure 1.2: *Typical graph of cell voltage versus discharge capacity. The area under the curve represents the specific energy of the material [2].*

In the case of an electrochemical cell, the theoretical energy of the overall process can be expressed by:

$$\Delta G = -nFE_{cell} \quad (1.5)$$

where n is the number of electrons transferred per mole of reactants, F is the Faraday constant (96490 C mol^{-1}) and E_{cell} is the voltage associated with the specific battery chemistry [2].

Another key property of an electrochemical cell is power. Power is the rate of energy conversion. High power devices are able to provide significant amount of energy in a short

period of time. Specific power or power density is the amount of power per unit of mass ($W\ kg^{-1}$) [1, 2].

In Figure 1.3, a Ragone plot, which allows the comparison of different devices based on their specific energy and specific power, is presented. This Ragone plot demonstrates different electrochemical systems in comparison to a combustion engine. Batteries are moderately high in energy density when compared to the internal combustion engine. On the other hand when it comes to power, batteries lag behind the internal combustion engine by quite a few orders of magnitude. Figure 1.3 also demonstrates capacitors and supercapacitors. A capacitor is a device used in electronic circuits to store charge temporarily. It usually consists of two metallic plates which are insulated with a dielectric. A supercapacitor is a capacitor with a higher energy density. When comparing batteries to capacitors and supercapacitors, it is clear that in the case of batteries, the energy density is superior by at least an order of magnitude. On the other hand, capacitors and supercapacitors have much larger specific power. Figure 1.3 also displays fuel cells which are devices that are similar to batteries in that both produce electricity via an electrochemical reaction except that fuel cells require a constant supply of fuel as opposed to batteries which are closed devices. Fuel cells have high energy density but have the lowest specific power out of all the different systems.

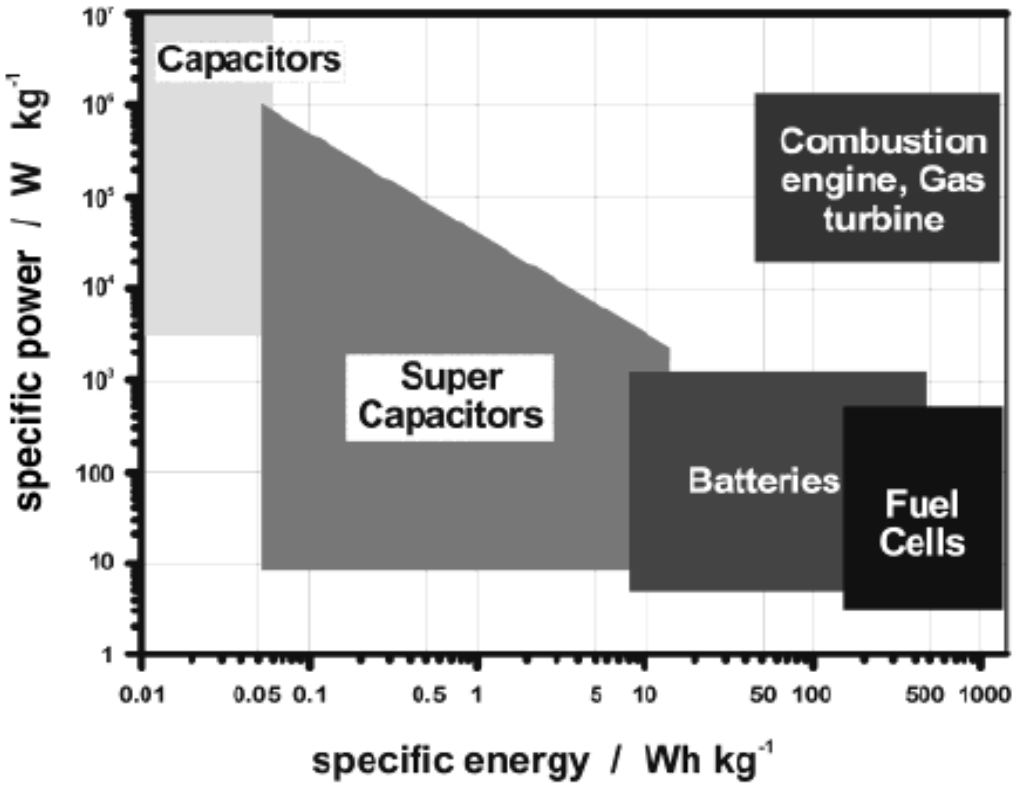

Figure 1.3*: Ragone plot demonstrating various electrochemical conversion systems compared to a combustion engine [2]*

In Figure 1.4, different rechargeable batteries are demonstrated with respect to their energy density and specific energy. The portable battery technologies that offer highest energy density at the moment are lithium-ion (Li-ion) based systems. These systems, more specifically the cathode materials, will be the main interest within this thesis and thus they will be described in greater detail.

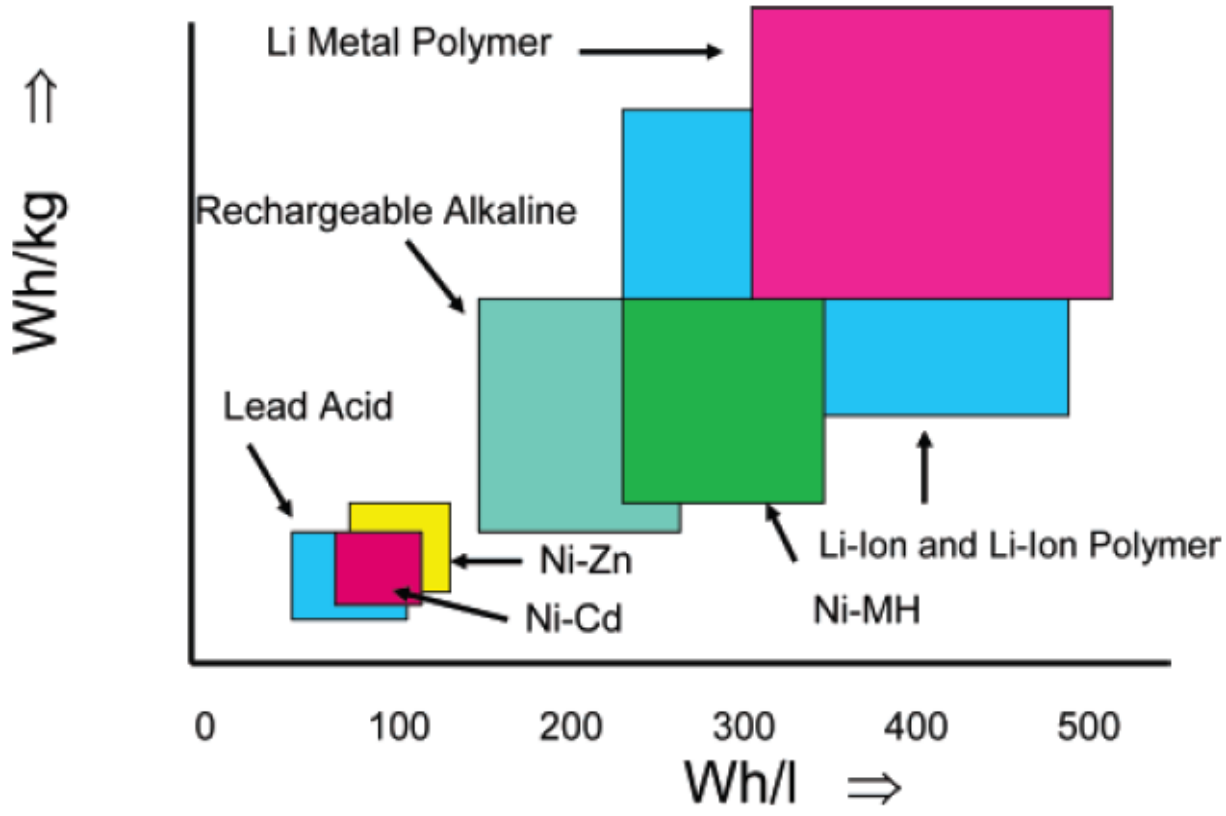

***Figure 1.4**: Specific energy and energy density of various secondary battery devices [2]*

1.2 Cathode materials for Li-ion batteries

The first lithium based battery was proposed by Whittingham in the 1970s. In this battery, the cathode material consisted of lithium titanium disulfide ($LiTiS_2$) and the anode material was lithium metal [3]. The cathode material has a layered structure such that the lithium can be extracted or inserted in between the layers of TiS_2. The system contained numerous issues that prevented widespread commercial production such as poor safety, due to high reactivity of the lithium metal as a rechargeable electrode, as well as loss of reversible capacity with cycling. Mizuchima et al. discovered lithium cobalt oxide ($LiCoO_2$) which due to the oxygen-cobalt

bonding, gave rise to higher operating voltage and since the product of voltage and capacity is energy density therefore the material had high energy density [4]. Sony commercialized $LiCoO_2$ based batteries with graphite as the anode in 1990. This was the first Li-ion battery and at the moment it is still a popular battery chemistry for commercial applications [5]. In this work, emphasis will be focused on more recently discovered cathode materials namely $LiFePO_4$ and Li_2FeSiO_4. At the moment the main research interests of Li-ion technologies are reducing the cost of production, improvement safety and increasing cycle life. The future research direction would be developing stable Lithium-air battery systems as well as the development of sodium based batteries.

1.2.1 Olivine material

$LiFePO_4$ is compound that was reported for use in Li-ion batteries by Prof. Goodenough and coworkers in 1997 [6]. $LiFePO_4$ has an operating voltage of 3.45 V (versus Li/Li^+) with a flat charge/discharge profile. Typically, a sloping charge/discharge profile would suggest that the system does not go through a phase change i.e. one phase is present through the charge/discharge cycle. In the case of $LiFePO_4$, during charge/discharge two distinct phases of $LiFePO_4$ and $FePO_4$ are present leading to a flat charge/discharge profile [2]. The material also has the benefits of high theoretical capacity (170 mAh g^{-1}) and most importantly high thermal stability making it safe for use in many different electronic devices [7]. The crystal structure of $LiFePO_4$ is orthorhombic with a *Pnma* space group. It is composed of iron bonding with oxygen atoms in an octahedral coordination in addition to a tetrahedral phosphorus-oxygen bonding environment (Figure 1.5). The lithium atoms are linearly oriented along the b-axis. The specific area where

lithium atoms are located in the lattice is called the M1 site and the area of location of iron atoms is called the M2 site.

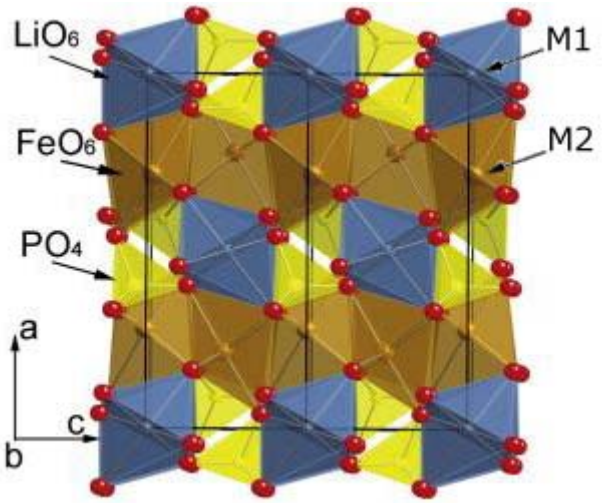

***Figure 1.5**: Crystalline structure of $LiFePO_4$ [14]*

The main issue with $LiFePO_4$ is its low intrinsic conductivity (10^{-9} S cm^{-1}) which prevents the extraction of the theoretical capacity at high discharge rates [8]. Different methods were proposed to overcome this problem. Various synthetic routes were developed which gave rise to nanomaterials with particle size in nanometer regime. Reducing particle size results in short diffusion paths for the electron and the lithium ion such that high capacity values can be achieved [9, 10]. Substitution of transition metals like niobium and zirconium instead of lithium in the M1 site also improved the performance of the material [11]. Another method that gave rise to high performance was the formation of a thin layer of amorphous carbon on the surface of the $LiFePO_4$ particle [12]. This method is called "carbon coating". Carbon coating is typically done by mixing $LiFePO_4$ with an organic carbon source. The mixture is then heated to high

temperatures, around 700 °C, under an inert atmosphere. The organic precursors decompose and form an amorphous carbon layer which adheres to $LiFePO_4$ particles creating an interconnected web like network which increases the overall conductivity of the material. In addition, the charge/discharge rate capability, in other words power, could be dramatically improved by starting with an off-stoichiometric synthesis to obtain a poorly crystallized layer of $Li_4P_2O_7$ on the surface of $LiFePO_4$ particles [13]. Over the past two decades $LiFePO_4$ was optimized to a point when one could extract almost theoretical capacity from it. This gave rise to many start-up companies who have commercialized the material for example, A123 Systems and Phostech Lithium to name a few.

1.2.2 Silicon based cathode

Li_2FeSiO_4 was first synthesized and characterized for Li-ion battery application by Nyten et al. [15]. This material is part of a more general family of lithium metal silicates or simply Li_2MSiO_4 (where M = Fe, Ni, Co, Mn). Li_2FeSiO_4 has many advantages such as low cost, an abundance of precursors as well as high theoretical capacity of 166 mAh g^{-1} for a one electron reaction. The operating voltage of Li_2FeSiO_4 is 2.8 V with a flat charge/discharge profile suggesting a two phase process electrochemistry. The main drawback of this material is poor conductivity which is on the order of 6×10^{-14} S cm^{-1}[16]. Li_2FeSiO_4 has many different structures, polymorphs, whose presence depends on the temperature used for its synthesis. For low temperature synthesis (400 °C), the crystallographic space group of the polymorph is $Pnm2_1$. At high temperature (900 °C) the polymorph is a member of the *Pmnb* space group. There are also numerous polymorphs that occur when the synthetic temperature is in between these

temperatures [17]. In all cases, the structure features silicon and iron which are connected to oxygen atoms in a tetrahedral coordination. The capacity typically obtained for synthesized Li_2FeSiO_4 is approximately 130 mAh g^{-1} [18, 19, 20]. This leaves a lot of room for improvement in the near future.

An interesting point to consider for Li_2FeSiO_4 is the possible removal of two lithium per molecule of Li_2FeSiO_4. In the case of iron, the oxidation of Fe^{3+}/Fe^{4+} occurs at a very high voltage which would not be suitable for the electrolyte due to the thermodynamic instability of the electrolyte. In the case of Li_2MnSiO_4, the second oxidation, Mn^{3+}/Mn^{4+}, occurs at a much more accessible voltage and could be a possible direction in the future [21].

1.3 Motivation and Goals

The work described in this thesis will be divided in two parts. The first part will investigate two different lithiation reactions of amorphous $FePO_4$ in order to obtain a pure phase of amorphous $LiFePO_4$. A detailed characterization for each step of the reaction was performed in order to understand the nature of obtained products. The initial goal of this work was to synthesize amorphous $LiFePO_4$ and to measure its electrochemical performance. It has been demonstrated that amorphous lithium phosphates are good lithium conductors [13]. Our idea was to synthesize amorphous $LiFePO_4$ and hope to obtain a material that would have high lithium mobility. The electronic mobility could be improved by adding a carbon coating. Overall, the newly synthesized material would benefit from high lithium and electron mobility which would give rise to high rate performance. Unfortunately, the synthesis described in the literature as well

as our attempts did not produce amorphous $LiFePO_4$; nonetheless interesting information was obtained about two specific reactions mechanisms. This work will be described in greater detail in chapter 3 and is the subject of an article recently published in the Journal of Power Sources.

The second objective of this thesis is the development of a novel synthetic method for the synthesis of Li_2FeSiO_4. This method required the use of low cost precursors and simple equipment in order to minimize the cost of production. The inspiration for this work was the possibility of creating a product that would deliver good electrochemical performance while being relatively inexpensive to produce. This work will be described in chapter 4.

The main goal of this master's degree was learning and acquiring as much knowledge as possible about the field of material science in order to push the boundaries of science a little further.

1.4 References

1. Peng, B.; Chen, J. *Coord. Chem. Rev.* **2009**, 253, 2805.
2. Winter, M.; Brodd, R., J. *Chem. Rev.* **2004**, 104, 4245.
3. Whittingham, M. S., *Science*, **1976**, 192, 1126.
4. Mizushima, K.; Jones, P. C.; Wiseman, P. J.; Goodenough, J. B., *Materials Research Bulletin*, **1980**, 15, 783.
5. Antolini, E., *Solid State Ionics,* **2004**, 170, 159.
6. Padhi, A. K.; Nanjundaswamy, K. S.; Goodenough, J. B., *J. Electrochem. Soc.*, **1997,** 144, 1188.
7. Takahashi, M.; Tobishima, S.; Takei, K.; Sakurai, Y., *Solid State Ionics*, **2002**, 148, 283.
8. Ting-Kuo Fey, G.; Chen, Y. G.; Kao, H.-M., *J. Power Sources*, **2009**, 189, 169.
9. Gao, F.; Tang, Z.; Xue, J. *Electrochimica Acta*, **2007**, 53, 1939.
10. Wang, L.; Huang, Y.; Jiang, R.; Jia, D., *Electrochimica Acta*, **2007**, 52, 6778.
11. Chung, S.-Y.; Bloking, J. T.; Chiang, Y.-M., *Nature Materials*, **2002**, 2, 123
12. Ravet, N.; Chouinard, Y.; Magnan, J. F.; Besner, S.; Gauthier, M.; Armand, M., *J. Power Sources*, **2001**, 97, 503
13. Kang, B.; Ceder, G., *Nature*, **2009**, 458, 190
14. Li, J.; Yao, W.; Martin, S.; Vaknin, D., *Solid State Ionics*, **2008**, 179, 2016
15. Nyten, A.; Aboumrane, A.; Armand, M.; Gustafson, T.; Thomas, *J. O. Electrochem. Commun.*, **2005**, 7, 156.
16. Dominko, R., *J. Power Sources*, **2008**, 184, 462.
17. Sirisopanaporn, C.; Boulineau, A.; Hanzel, D.; Dominko, R.; Budic, B.; Armstrong, A. R.; Bruce, P. G.; Masquelier, C., *Inorg. Chem*., **2010**, 49, 7446.

18. Dominko, R.; Conte, D. E.; Hanzel, D.; Gaberscek, M.; Jamnik, J., *J. Power Sources*, **2008**, 178, 842.

19. Huang, X.; Li, X.; Wang, H.; Pan, Z.; Qu, M.; Yu, Z., *Solid State Ionics*, **2010**, 181, 1451.

20. Li, L.; Guo, H.; Li, X.; Wang, Z.; Peng, W.; Xiang, K.; Cao, X., *J. Power Sources*, **2009**, 189, 45.

21. Kuganathan, N.; Islam, M. S., *Chem. Mater*. **2009**, 21, 5196.

Chapter 2

Experimental Procedures

2.1 Methods of synthesis

2.1.1 Synthesis of $LiFePO_4$

Two methods were employed to synthesize $LiFePO_4$. The first method involved dissolving $FeSO_4.7H_2O$ and $NH_4H_2PO_4$ (Aldrich) in distilled water with equimolar concentrations of 0.01 M. This was followed by the addition of H_2O_2 (50% weight, Aldrich) in a molar ratio of 1.1:2 for H_2O_2:$FeSO_4.7H_2O$. This produced a yellow precipitate which was then centrifuged and washed with distilled water. The yellow precipitate was later characterized as amorphous $FePO_4.xH_2O$ (a-$FePO_4.H_2O$). The product was dried in an oven at 60 °C under air. A dehydrated sample (a-$FePO_4$) was obtained by further drying the powder at 400 °C for 24 hours. The lithiation step, to produce $LiFePO_4$, was performed using lithium acetate as the lithium source (molar ratio of 1.2:1 for Li:Fe) and ascorbic acid (VC) as the reductant (molar ratio of 0.6:1 for VC:Fe). Lithium acetate and ascorbic acid were first dissolved in isopropyl alcohol (IPA) followed by the addition of either the hydrated or the dehydrated a-$FePO_4$. In both cases the solution was vigorously stirred and kept at 60 °C with an overflow of N_2 gas. After 5 hours, the product was centrifuged and dried in an oven at 60 °C under vacuum. The synthesized powder was thermally treated in a tubular furnace at 600 °C for 3 hours under an Ar/H_2 (5%) atmosphere. This synthetic route was based on the method previously suggested by Wang et al. in [1].

The second $LiFePO_4$ synthesis involved 0.03M equimolar aqueous solution of $Fe(SO_4)_2(NH_4)_2.6H_2O$ and $NH_4H_2PO_4$ (Aldrich). The addition of 2 ml of 50% weight H_2O_2 to this solution instantly formed a yellowish precipitate which after characterization proved to be a-$FePO_4.xH_2O$. The precipitate was washed and dried at 60 °C. The dehydrated sample was obtained, similarly as before, by treating the product at 400 °C for 24 hours. The synthesized hydrated and dehydrated a-$FePO_4$ were lithiated in a 1M solution of lithium iodide (molar ratio of 15:1 for Li:Fe) in acetonitrile (Fisher). The solution was vigorously stirred for 24 hours and the lithiation process was performed in an argon filled glove box to avoid any oxidation of iodide to iodine. Finally the product was filtered, washed with acetonitrile and dried at 60 °C in a vacuum oven. In order to obtain a crystalline product, a thermal treatment was performed at 600 °C for 3 hours under Ar/H_2 (5%) atmosphere. For both synthetic procedures all the samples were kept in an argon filled glove box to avoid any kind of oxidation. This method of synthesis was proposed by Prosini et al. in [2].

2.1.2 Synthesis of Li_2FeSiO_4

A solid-state reaction of stoichiometric amounts of Li_2CO_3 (Limtech, Québec), Fe_2O_3, fumed SiO_2 and ß-lactose (Aldrich) were used to prepare Li_2FeSiO_4. The reactants were ball milled using a SPEX SamplePrep 8000D mill with stainless steel vials containing two stainless steel balls (½ inch in diameter) and 15 ml of acetone. The ball to sample mass ratio for the milling was ~7:2. The milling consisted of for 4 cycles of 45 minutes followed by 15 minutes of rest. A red slurry like composition was obtained and the mixture was then left to dry under ambient conditions. The dried powder was then placed in porcelain crucibles and thermally

treated in a tubular furnace at temperatures ranging from 600 °C to 900 °C for 3 hours under a N_2 atmosphere. The resulting powder was of gray color. The powder was milled using a planetary mill (Fritsch). Approximately 1.75 grams of powder and 25 ml of IPA was milled in a 250 ml Syalon (Si_3N_4) container using 100 g of Syalon milling media 5 mm in diameter. The operating speed was set to 600 rpm. In order to have a material with equally distributed particle size, the powder was passed through a 38 μm sieve. The material was then carbon coated by suspending the synthesized Li_2FeSiO_4 in water containing 10% weight ß-lactose. The solution was stirred at room temperature until all the water was evaporated. The dried powder was then thermally treated at 600 °C for 1 hour to decompose the ß-lactose into a conductive carbon layer on the surface of the Li_2FeSiO_4 particles. The color of the carbon coated powder was black.

2.2 Characterization

2.2.1 Powder X-ray Diffraction

One of the key characterization techniques when working with crystalline materials is X-ray diffraction. The diffraction pattern results due to the interaction of X-rays with the electrons of the atoms present in the crystalline lattice. The arrangement of the atoms within the lattice give rise to constructive or destructive interference of scattered X-rays [3, 4]. The selection criteria for the interference can be obtained from Bragg's Law:

$$n\lambda = 2d \sin(\theta) \tag{2.1}$$

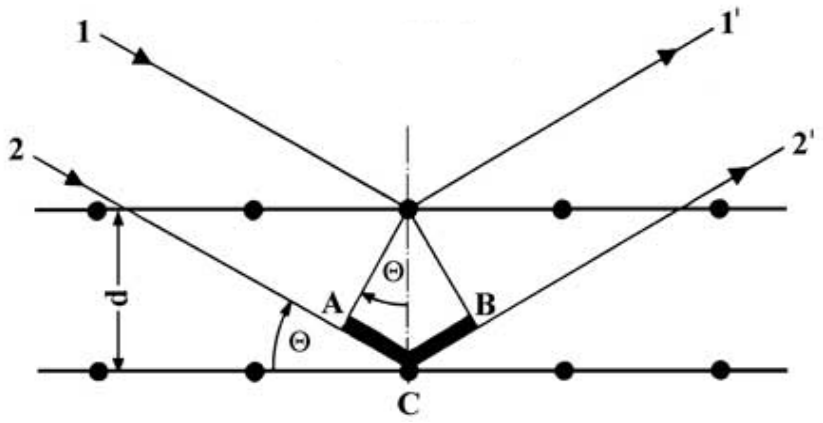

***Figure 2.1**: Schematic illustration of Bragg's Law [5]*

where θ is the angle formed between the atomic layer and the incoming X-ray, d is the distance between two layers of atoms, n is an integer and λ is the wavelength of the ray. The two rays (1 and 2) come in with the same phase and parallel (Figure 2.1). Beam 1 strikes the top atomic layer and gets reflected. Beam 2 strikes the bottom layer and gets reflected off point C. Beam 2 has to travel an additional distance from A to C to B. The distance ACB is equal to 2dsin(θ). The distance ACB or 2dsin(θ) has to be an integer of the wavelength (nλ = ACB), in order for the two rays to continue travelling in phase and produce constructive interference. In the case were ACB is not an integer of the wavelength, destructive interference will occur. The powder sample is scanned throughout the desired range of angles and the data is collected [3, 4].

Figure 2.2 is a representation of a typical powder X-ray diffractometer. The apparatus contains an X-ray tube, a sample holder and a detector. The X-ray tube contains a cathode and an anode which are kept at a large potential difference. The cathode is composed of a tiny filament

which is heated when high current is applied. Electrons from the cathode are then liberated via thermionic emission and accelerate in the electric field towards the anode. The incident electron can knock out an electron from the target atom inner shell such that another electron sitting in an outer shell has to fill in the vacancy. During the transition of the electron from the outer to the inner shell a photon is emitted in the X-ray region [3, 4, 5]. An electrostatic interaction can occur between an incident electron that passes sufficiently close to the atomic nucleus of the metal anode such that the electron is decelerated resulting in emission of a photon in the X-ray region; this process is called brehmsstrahlung (breaking radiation). The X-rays travel from the tube to the sample, where scattering occurs and the X-rays are collected by the detector [3, 4].

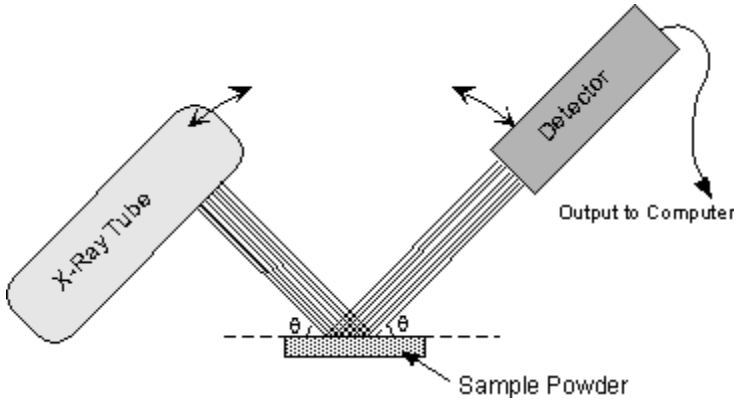

***Figure 2.2**: Illustration of powder X-ray diffractometer[6]*

The synthesized samples were analyzed by powder X-ray diffraction (XRD, Bruker D8 Advance) with Cu Kα radiation. The analysis were performed with a step size of 0.05° and a step time of 9 seconds in the diffraction angle range of 2θ from 15 to 70° (where 2θ is the angle between the sample and the incoming ray multiplied by two). Sample preparation included

grinding samples to powder form using a mortar and pestle and mounting the powder in specifically designed holders.

2.2.2 Scanning Electron Microscope

Scanning Electron Microscope (SEM) was used in order to study the morphology of the synthesized material. SEM functions similarly to a regular microscope, except that instead of light, electrons are used. An electron gun produces a stream of electrons thermionically which are directed towards the anode (target) that contains a small aperture (see Figure 2.3). The electrons which pass through the aperture are then focused into a beam using several circular electromagnets. The sample is placed on the stage which is located at the bottom of the column. The beam of electrons scan the area around the sample. The electrons are either absorbed by the sample or they are scattered. The scattered electrons are called secondary electrons. These secondary electrons are collected by a detector which converts the signal and a detailed image of the sample is obtained [3, 4, 7]. Samples analyses were performed at voltages from 5 to 10 kV with a working distance of 15 mm. A Hitachi S-4300 was used to collect all the SEM data. All the samples were analyzed in the Laboratory of Microfabrication at the École Polytechnique de Montréal.

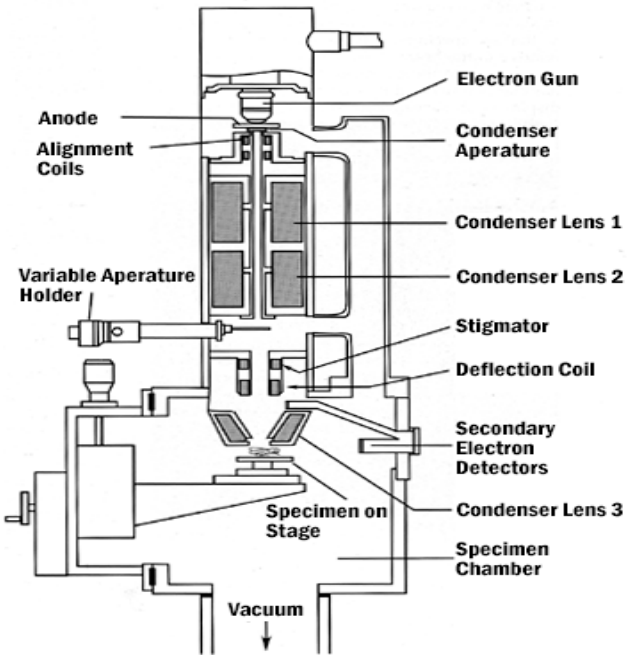

***Figure 2.3**: Diagram of various components inside the SEM [8]*

2.2.3 Thermogravimetric analysis and Differential scanning calorimetry

Thermogravimetric analysis (TGA) is a technique that is performed to determine the change in weight of a sample with respect to change in temperature. This technique investigates the thermal stability of the material as well as the reactivity of the sample in a specific atmosphere. Typically, a sample is placed in a platinum or alumina crucible and the furnace is then flushed with the desired gas. The temperature in the furnace is then increased linearly and the change in weight is recorded throughout the experiment [3].

Differential scanning calorimetry (DSC) is a thermoanalytical technique that measures the difference in the amount of heat required to increase the temperature of the sample in

comparison to a reference. There, a reference crucible is placed on an adjacent holder to the sample crucible. The system is then flushed with a desired gas and heated. DSC is useful to measures glass transitions, crystallizations, fusion temperatures as well as a variety of other chemical reactions [3].

In our laboratory, a TGA/DSC measurements was performed using a TA Instrument SDT Q 600 apparatus. The advantage of such apparatus is that both the TGA and DSC measurements can be performed simultaneously. The samples were analyzed under helium atmosphere. The heating rate varied from 5 to 15 °C min^{-1}. The samples were heated from room temperature to temperatures typically above 700°C. The sample size was varied from approximately 30 to 40 mg.

2.2.4 Mössbauer Spectroscopy

Mössbauer spectroscopy is a technique used to identify the chemical, structural and magnetic properties of a material. It is used in many areas of science such as physics, metallurgy, chemistry and even biology. In 1957, Rudolf Mössbauer discovered that when an atom is in a solid matrix, the effective mass of the nucleus becomes much larger such that when γ-rays are directed at the system, a recoil free emission or absorption (resonance) can be observed. This phenomenon was named the "Mössbauer effect" for which Rudolf Mössbauer won the Noble Prize in Physics in 1961 [3, 4, 9].

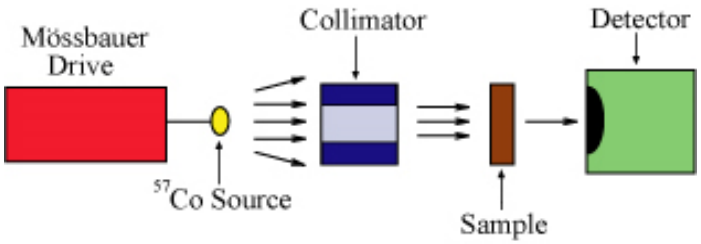

***Figure 2.4**: Diagram of a typical setup up for Mössbauer Spectroscopy [10]*

The set up of a Mössbauer experiment is demonstrated in Figure 2.4. The apparatus is composed of a Mössbauer drive, source, collimator, sample holder and a detector. The Mössbauer drive oscillates the source such that the emitted γ-rays have a range of energies due to the Doppler effect. The source in the setup used for the experiments in this thesis is ^{57}Co which decays to ^{57}Fe and emits a γ-ray. The collimator has the role of focusing the γ-rays into a narrow beam. Next, the γ-rays reach the sample and the detector collects the intensity of the transmitted beam. When the γ-rays are in resonance with the sample energy levels, absorption occurs which is noted with a dip on the spectrum. The number of peaks (dips), their position and their intensities present information about the samples absorbing nuclei [3, 4].

There are three important nuclear interactions that can be observed between the incoming γ-rays and the sample. All the three interactions are demonstrated in Figure 2.5. The first interaction is the Isomer Shift (IS) which occurs due to changes in the electron density of the s orbital when incorporated in a different lattice relative to the source [9, 10]. Because of these differences in s-electron environment a shift in the Mössbauer spectrum is observed (Figure 2.5 in blue). The second interaction is the Quadrupole Splitting (QS) which occurs when the nuclei is

in a state such that the charge distribution is non-spherical which in turn gives rise to an asymmetric electric field at the nucleus [9, 10]. This gives rise to energy level splitting (Figure 2.5 in red). The third interaction is the Magnetic or Hyperfine Splitting (Figure 2.5 in green). Here, the nuclear magnetic moment interacts with a magnetic field which causes energy level splitting [3, 4, 9, 10].

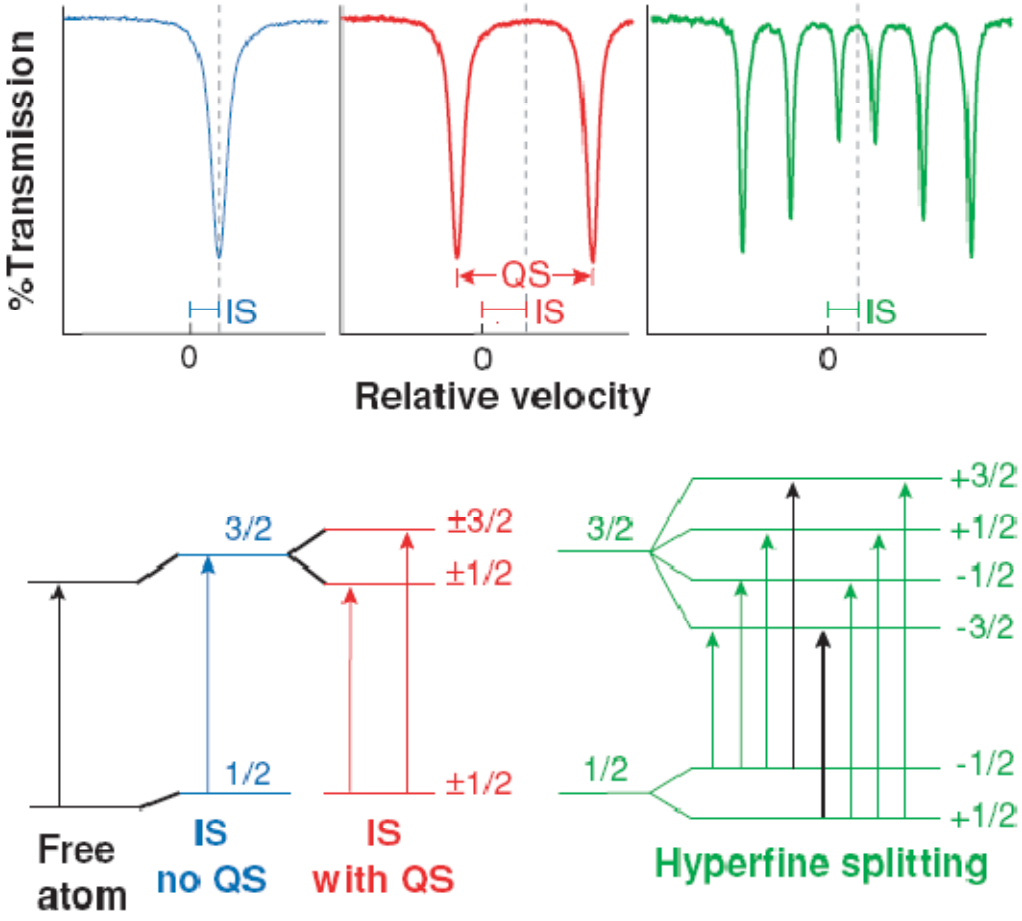

***Figure 2.5**: Three important interactions observed when using Mössbauer spectroscopy [11]*

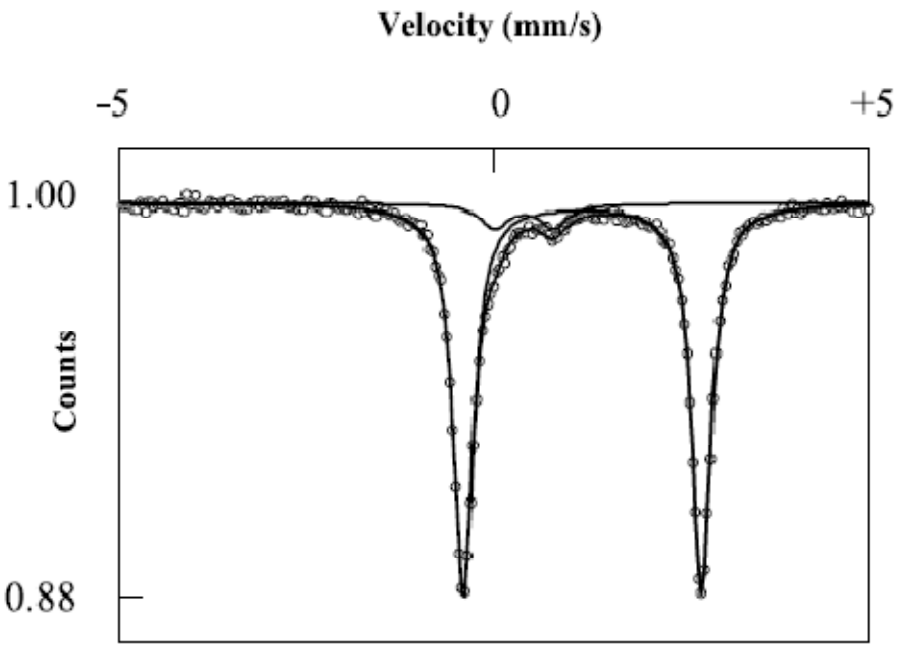

Figure 2.6: *Typical Mössbauer spectrum for $LiFePO_4$ with some impurities [12]*

An example of a typical Mössbauer spectrum for $LiFePO_4$ is demonstrated in Figure 2.6. Two sets of doublets are observed. The more prominent doublet has an IS of 1.20 mm s^{-1} and a QS of 2.96 mm s^{-1} suggesting the presence of $LiFePO_4$. For olivine type crystalline $LiFePO_4$ values of IS that were reported are in the range of 1.20-1.25 mm s^{-1} and 2.95-2.98 mm s^{-1} for QS [12]. The second doublet has an IS of 0.47 mm s^{-1} and a QS of 0.74 mm s^{-1}, which is most likely an Fe^{3+} impurity. Generally, IS values lower than 0.5 mm s^{-1} indicate the presence of an Fe^{3+} and values of IS higher than 0.9 mm s^{-1} indicate the presence of Fe^{2+} species. Iron atoms can be in both oxidation states (Fe^{2+} and Fe^{3+}) when values of IS are in between 0.5 and 0.9 mm s^{-1}[11]. The QS values measure distortion around the Fe atom. The larger the QS value, the more distorted is the coordination polyhedron surrounding the iron atom [10, 11]. The area under the curves indicates the amount of specific material present in the sample. In this case the prominent

doublet ($LiFePO_4$) has an area of 92% and the smaller doublet (Fe^{3+} species) has an area of 8% [12].

The samples analyzed in this thesis, typically 30 mg, were mixed with boron nitride and all the spectras were collected at room temperature. A nonlinear least-squares minimization was used to fit the spectra to a sum of Lorentzian lines each representing a peak on the spectrum. In the case of significant disorder, line broadening was modeled using a Pseudo-Voigt lineshape. All the samples were analyzed in Prof. Dominic Ryan's laboratory in the Physics Department at McGill University.

The use of Mössbauer spectroscopy is a key tool for studying amorphous compounds. This is due to the fact that powder X-ray diffraction does not provide any information about these poorly crystallized materials. In this thesis, amorphous $FePO_4$ was synthesized, then lithiated in solution and each step of the reaction was studied using Mössbauer spectroscopy in order to understand the mechanism of the reaction. This will be discussed in greater detail in Chapter 3.

2.2.5 Electrochemical analysis

The synthesized cathode materials ($LiFePO_4$ and Li_2FeSiO_4) were evaluated electrochemically in coin cells (Figure 2.7). The cells consisted of an anode, in this case lithium metal, a separator and a cathode. The active material (50% by weight) was mixed with a

previously prepared mixture containing polyoxyethylene (POE, 400000 g mol^{-1}) and acetylene black (42% and 8% respectively). The role of POE and acetylene black mixture is to connect each particle and bind them together such that electrons can be transported to and from the current collector. The components were mixed with a mortar and pestle and acetonitrile was slowly added to dissolve the POE. Once a "paint" like consistency was obtained, the mixture was deposited on a stainless steel current collector. The electrodes were then left to dry under vacuum, weighed and brought into an Ar filled glove box [13].

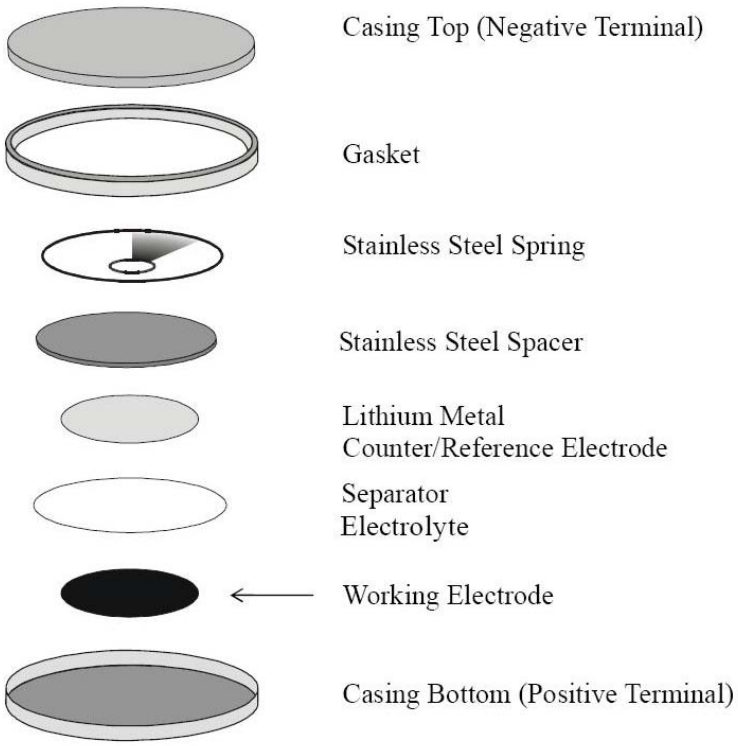

***Figure 2.7**: Components of a standard laboratory coin cell*

To complete the construction of the electrochemical cell, a separator/electrolyte was prepared by dissolving POE (7000000 g mol^{-1}) and LiTFSi (75% and 25% weight) in acetonitrile in a dry air glove box. The solvent was degassed under vacuum and then slowly evaporated under dry air until a thin white colored film was obtained. The film was cut into disks 13 mm in diameter. The cells were assembled in an argon filled glove box. A hand powered press was used to seal the top and bottom casings together [13].

The cells were cycled on a VMP electrochemical station (Biologic, France) with the EClab software. The temperature of operation was 80 °C. For both materials ($LiFePO_4$ and Li_2FeSiO_4), the cycling cut off voltage was set from 2.0 V to 4.0 V, due to the redox couple of $Fe^{2+/3+}$ that occurs at 3.45 V for $LiFePO_4$ and 2.8 V for Li_2FeSiO_4 vs Li/Li^+. Galvanostatical cycling was performed typically with current equal to 17 mA g^{-1} (17 mA per gram of active material) unless specified otherwise. The current rate was chosen such that a full cycle (charge and discharge) could be performed in ~20 hours. Normally applying a high current leads to smaller capacity and a lower current leads to higher capacity due to the system being close to an equilibrium state.

Figure 2.8 demonstrates an example of a typical charge/discharge curve of $LiFePO_4$ with cut off voltage of 2.75 and 4 V. The charge cycle is the top curve and the discharge is the bottom line. The active weight and the applied current are needed in order to evaluate the capacity of the obtained material. For example, if a coin cell containing 1 gram of $LiFePO_4$ is charged with applied current of 8.5 mA for 20 hours then the full (theoretical) capacity of 170 mAh g^{-1} should

be obtained (8.5 mA*20 h/1 g = 170 mAh g^{-1}). By plotting the voltage versus the capacity a similar plot as in Figure 2.8 can be obtained. Since the charge reaction is reversible, a plot of capacity for a full charge or discharge versus cycle number can be obtained to evaluate the performance and stability of the material over many cycles.

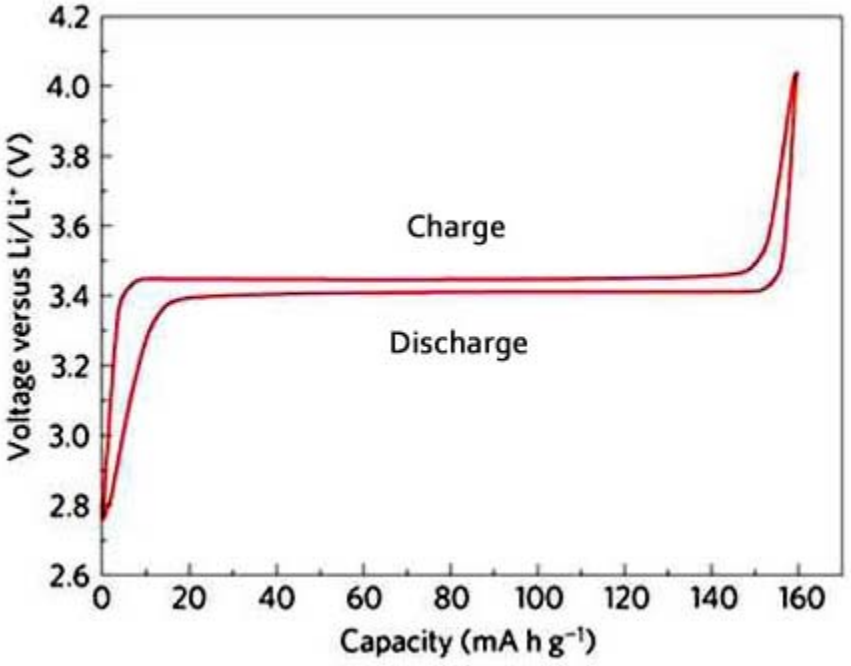

***Figure 2.8**: A typical charge and discharge curve of $LiFePO_4$ at a current of 8.5 mA g^{-1} [14]*

2.3 References

1. Wang, B.; Qiu, Y.; Ni, S., *Solid State Ionics*, **2007**, 178, 843.
2. Prosini, P. P.; Carewska, M.; Scaccia, S.; Wisniewski, P.; Passerini, S.; Pasquali, M., *J. Electrochem. Soc.*, **2002**, 149, 886.
3. Skooq, D. A.; Holler, F. J.; Nieman, T. A., *Principle of Instrumental Analysis*, **1997**, Thomson Brooks/Cole.
4. Laider, K. J.; Meiser, J. H.; Sanctuary, B. C. *Physical Chemistry*, **2002**, Thomson Brooks/Cole.
5. Schlotz, R.; Uhlig, S., *Introduction to X-ray Fluorescence Analysis*, **2006**, Bruker AXS GmbH.
6. Nelson, S. A., *Xray Crystallography*, Tulane University, **2010**.
7. Goldstein, J.; Newbury, D.; Joy, D.; Lyman, C.; Echlin, P.; Lifshin, E.; Sawyer, L.; Michael, J., *Scanning Electron Microscopy and X-Ray Microanalysis*, **2003**, Springer.
8. Nessler, R., *Scanning Electron Microscopy*, University of Iowa, **2010**
9. Maddock, A. G., *Mössbauer Spectroscopy: Principles and Applications*, **1997**, Woodhead Publishing.
10. Dyar, M. D., *Mössbauer Spectroscopy*, Mount Holyoke College, **2010**
11. Dyar, M.; Agresti, D. G.; Schaefer, M. W.; Grant, C. A.; Slute, E. C., *Annu. Rev. Earth Planet. Sci.*, **2006**, 34, 83
12. Prince, A. A. M.; Mylswamy, S.; Chan, T. S.; Liu, R. S.; Hannoyer, B.; Jean, M.; Shen, C. H.; Huang, S. M.; Lee, J. F.; Wang, G. X., *Solid State Commun.*, **2004**, 132, 455.
13. Zaghib, K.; Ait Salah, A.; Ravet, N.; Mauger, A.; Gendron, F.; Julien, C. M., *J. Power Sources,* **2006**, 160, 1381.

14. Dreyer, W.; Jamnik, J.; Gulhke, C.; Huth, R.; Moskon, J.; Gaberscek, M., *Nature Materials,* **2010**, 9, 448

Chapter 3

Characterization of two lithiation reactions starting with an amorphous $FePO_4$ precursor

K. Galoustov[1], M. Anthonisen[2], D. H. Ryan[2], D. D. MacNeil[1]

1. Département de chimie, Université de Montréal, Montréal, QC, H3T 1J4, Canada
2. Department of Physics, McGill University, Montreal, QC, H3A 2T8, Canada

Chapter 3 consists of an article published in the Journal of Power Sources. The article was prepared by the author under the supervision of Dr. MacNeil. The Mössbauer experiments were performed by M. Anthonisen under the supervision of Dr. Ryan at McGill University.

Abstract

$LiFePO_4$ was prepared using two synthetic routes which involved the precipitation and lithiation of an amorphous $FePO_4$ precursor followed by a thermal treatment. Both hydrated and dehydrated $FePO_4$ were used. The XRD patterns confirm the amorphous nature of both the precipitated and the lithiated product, while a crystalline $LiFePO_4$ product is obtained after thermal treatment. Mössbauer spectroscopy was used to analyse the oxidation state of iron during various stages of the reaction. The Mössbauer data demonstrates a large amount of Fe^{3+} ions in the lithiated samples which suggest that the lithiation reaction does not go to completion.

Therefore, the formation of $LiFePO_4$ may be in part associated with the thermal treatment and not the lithiation step.

Keywords *– Lithium-ion battery, amorphous $FePO_4$, Mössbauer spectroscopy, lithiation*

3.1 Introduction

Lithium ion batteries play an important role in various portable electronic devices. Numerous cathode materials have been proposed for these batteries, including lithium iron phosphate. $LiFePO_4$ can provide increased thermal stability, high theoretical capacity, low cost precursors and environmental friendliness over other commercial cathode materials. A variety of different synthetic routes have been developed for $LiFePO_4$, including solid state reactions [1, 2], microwave assisted methods [3], hydrothermal conditions [4, 5] and many others [6, 7, 8]. Lithium can be extracted from $LiFePO_4$ and inserted into $FePO_4$ at a flat voltage potential of 3.5 V versus lithium metal. However, a major disadvantage of pure $LiFePO_4$ can be attributed to its poor electronic conductivity which is on the order of 10^{-9} S cm^{-1} [9, 10]. One of the strategies to overcome this problem is to use nanosize material. One of the methods to achieve these nanoscale dimensions is by precipitating amorphous nanosized $FePO_4$ which can later be lithiated and thermally treated to obtain crystalline $LiFePO_4$ with small particle size [11, 12]. In this work, we present a detailed characterization of the reaction mechanism of two previously established synthesis routes that use amorphous $FePO_4$ (a-$FePO_4$) as a precursor. The a-$FePO_4$ is chemically lithiated and thermally treated to give rise to $LiFePO_4$ with high performance.

The first synthetic method (S1 in Figure 3.1) involves the precipitation of an amorphous $FePO_4.xH_2O$ material from a solution of $FeSO_4.7H_2O$ and $NH_4H_2PO_4$ [11]. Lithiation was performed using lithium acetate and ascorbic acid at a temperature of 60 °C. The product from the lithiation reaction was then heated to obtain $LiFePO_4$. The second synthesis (S2 in Figure 3.1) involves the precipitation of an amorphous $FePO_4.xH_2O$ from a solution of $Fe(SO_4)_2(NH_4)_2.6H_2O$ and $NH_4H_2PO_4$ [12]. The lithiation reaction was carried out using lithium iodide. The product was then heated to obtain crystalline $LiFePO_4$. In this investigation we used both hydrated and dehydrated amorphous $FePO_4$ during the lithiation reaction to determine the effect of the presence of water on the purity and performance of the resultant product. The product of each step within the synthesis was fully characterized using XRD and Mössbauer spectroscopy. Electrochemical tests were performed to confirm the presence and performance of the synthesized $LiFePO_4$.

3.2 Experimental Methods

3.2.1 Preparation

An aqueous solution of 0.01 M of $FeSO_4.7H_2O$ and $NH_4H_2PO_4$ (Aldrich) was prepared in distilled H_2O. H_2O_2 (50% by weight, Aldrich) was added to the solution until a molar ratio of 1.1:2 for H_2O_2:$FeSO_4.7H_2O$ was obtained. This resulted in the formation of a yellowish precipitate that was later found to be amorphous iron phosphate (a-$FePO_4.xH_2O$ denoted as FP1) through a combination of XRD and spectroscopic methods. The sample was then centrifuged, washed with distilled water and dried in an oven at 60 °C. A dehydrated sample (FP2) was obtained by heating FP1 in air at 400 °C for 24 hours. To synthesize $LiFePO_4$ from FP1 and FP2

a lithiation reaction was performed by adding FP1 or FP2 to a stirred solution of lithium acetate and ascorbic acid (VC) (molar ratio of Fe:Li:VC = 1:1.2:0.6) dissolved in iso-propyl alcohol (IPA) similarly to what is described in reference [11]. The sample was stirred for 5 hours at 60 °C under an overpressure of dry nitrogen. The product (denoted as L1 and L2 respectively), was then centrifuged, washed with iso-propyl alcohol and dried in an oven at 60 °C under vacuum. The obtained powder was heated to 600 °C for 3 hours under an Ar/H_2 (5%) atmosphere to obtain the crystallized product (R1 and R2 respectively). The reaction scheme for this preparation method (S1) is shown in Figure 3.1.

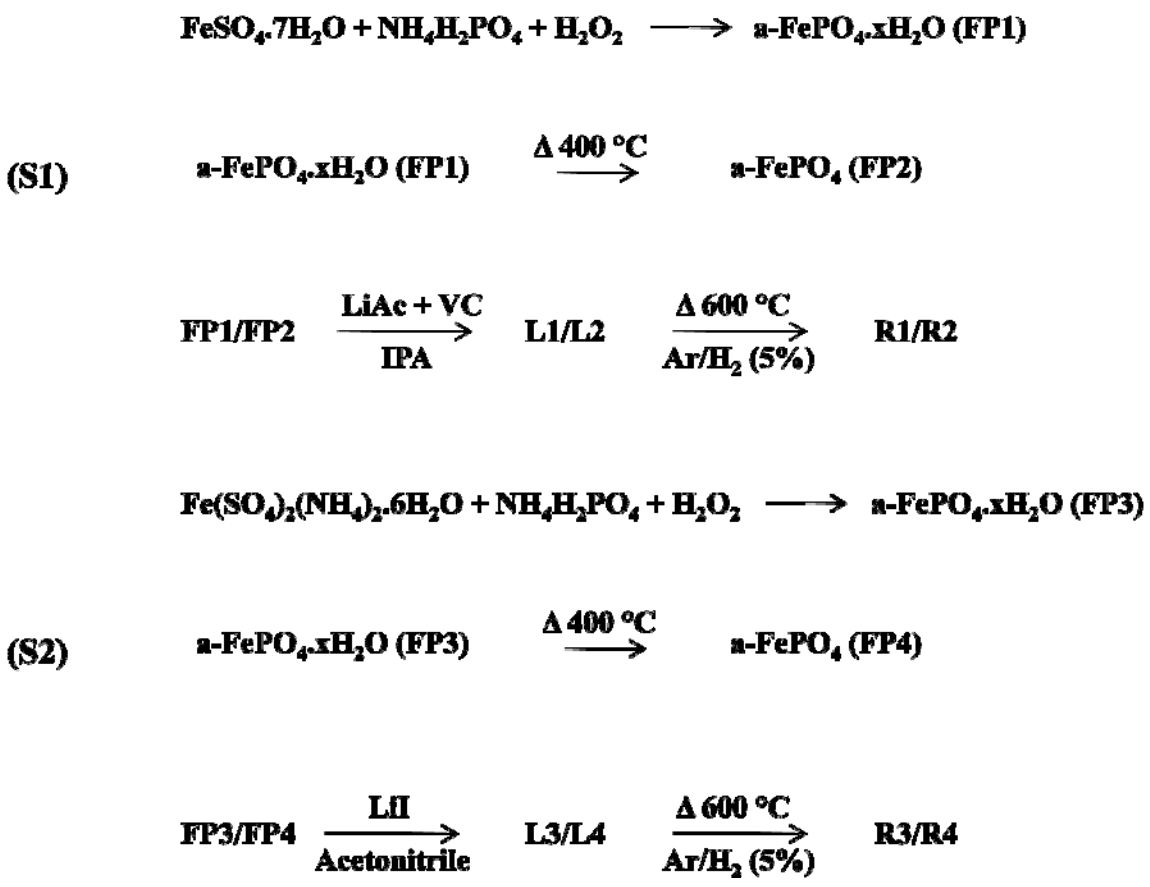

***Figure 3.1**: Schemes 1 and 2 of the performed synthesis*

The second reaction scheme (S2) is also described in Figure 3.1 and consisted of mixing a 0.03 M equimolar aqueous solution of $Fe(SO_4)_2(NH_4)_2.6H_2O$ and $NH_4H_2PO_4$ (Aldrich) together. The addition of 2 ml of 50 wt% H_2O_2 initiated the precipitation of a yellowish precipitate that was found to be amorphous iron phosphate (a-$FePO_4.xH_2O$ denoted as FP3). The sample was centrifuged, washed with distilled water and dried at 60 °C. A dehydrated sample (denoted as FP4) was obtained via thermal treatment of FP3 at 400 °C under air for 24 hours. The sample, FP3 or FP4, was then suspended in a 1 M solution of LiI in acetonitrile for 24 hours (molar ratio of Li:Fe = 15:1). The reaction was performed in an argon filled glove box to avoid oxidation of LiI. The product was filtered, washed with acetonitrile and dried at 60 °C under vacuum to obtain L3 and L4 respectively. A final thermal treatment to obtain a crystalline product was performed by heating the powder to 600 °C for 3 hours under Ar/H_2 (5%) to obtain R3 and R4 respectively.

3.2.2 Characterization

The thermogravimetric (TGA) and differential scanning calorimetry (DSC) analyses were performed using a SDT600 from TA instruments. The heating rate was 5 °C min^{-1} and the experiments were performed with a flowing He carrier gas. XRD analyses of the synthesized materials were performed on a Bruker D8 advance diffractometer using Cu Kα radiation. Mössbauer spectra were obtained using a 50 mCi ^{57}CoRh source mounted on a constant-acceleration spectrometer calibrated with α-Fe foil at room temperature. Samples weighing approximately 25-35 mg were mixed with boron nitride powder and spectra were collected at room temperature. A nonlinear least-squares minimization routine was used to fit the spectra to a

sum of Lorentzian lines. Where significant disorder was present, the resulting line broadening was modeled using a Pseudo-Voigt lineshape. Isomer shifts are given relative to the centre of the α-Fe spectrum.

Electrochemical evaluations on the synthesized $LiFePO_4$ were performed by combining $LiFePO_4$ (50% by weight) with a mixture of poly(ethylene oxide) (PEO) and KJ-Black carbon black (42% and 8% by weight respectively) following the procedure described previously [13]. This mixture was mixed with a mortar and pestle in acetonitrile to obtain a slurry. After well mixing, the slurry was deposited on a stainless steel current collector. The electrode was then left to dry overnight to evaporate the acetonitrile. The separator/electrolyte was prepared by mixing lithium bistrifluoromethanesulfonamide (LiTFSi) and POE (25% and 75% by weight respectively) in acetonitrile. The acetonitrile was slowly evaporated under dry air and the resultant polymeric film was cut into disks 13 mm in diameter. Standard 2032 coin-hardware (Hohsen) was used to test the electrochemical characteristics of these samples using lithium metal as both counter and reference electrode. Cells were assembled in argon filled glove box and the electrochemical evaluations were performed at 80 °C on a VMP electrochemical station (Biologic, France) with the EClab software. The cell was cycled galvanostatically with cut-off voltage of 2.0 and 4.0 V vs Li/Li^+ at a current equal to a rate of C/10.

3.3. Results and Discussion

All XRD patterns obtained during the investigation are summarized in Figure 3.3. Clearly both the as-synthesized $FePO_4.xH_2O$ (FP1 and FP3) materials and the dehydrated samples (FP2

and FP4) are amorphous. TGA-DSC data for FP1 and FP3 are presented in Figure 3.2. The data demonstrate a continuous weight loss until 500 °C of approximately 24% which can be associated with loss of water as reported previously [11,12]. The weight loss, at approximately 550 °C can be associated with the decomposition of co-precipitated ferric sulphate as described previously in [14].

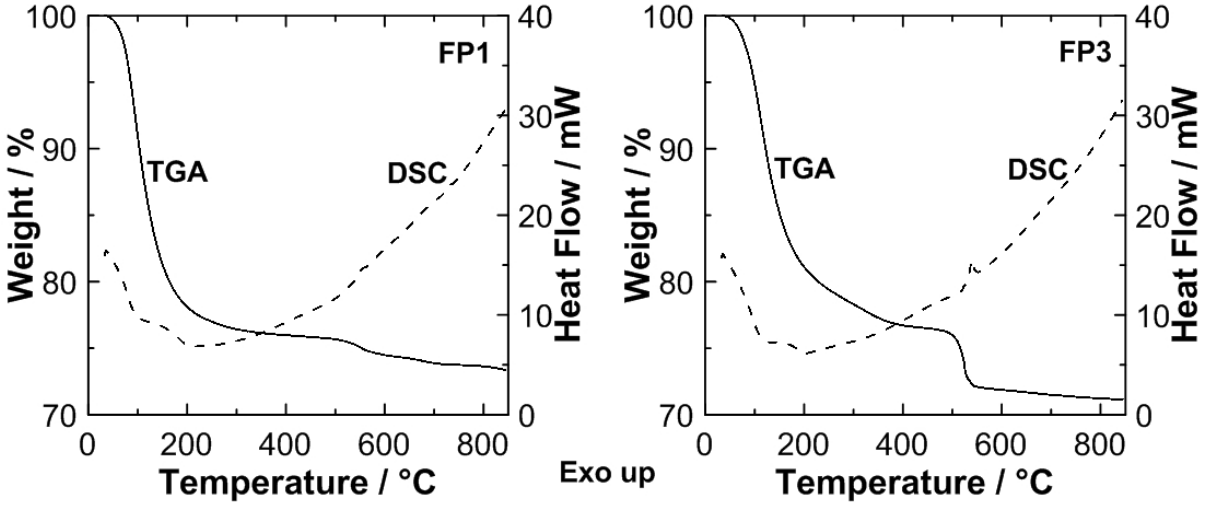

***Figure 3.2**: TGA-DSC for the synthesized amorphous $FePO_4$ by scheme 1 (FP1) and by scheme 2 (FP3). The data were collected at a heating rate of 5°C min^{-1} under helium.*

The goal of this study was to investigate the "so-called" amorphous intermediate sample (L1 to L4, in Figure 3.3) described by the previous reports as amorphous $LiFePO_4$ [11,12]. The amorphous nature of the samples after the lithiation step by XRD is shown in Figure 3.3 for samples L1 through to L4. Clearly, the amorphous nature of the samples is conserved through the various procedures except for L3 which contains a significant amount of a poorly crystallized

Li_3PO_4 impurity. Following thermal treatment at 600 °C under Ar/H_2 (5%), the products R1, R2 along with R4 demonstrate crystalline $LiFePO_4$ without any impurities. In the case of R3, a mixture of Li_3PO_4 and $LiFePO_4$ is obtained. Thus, both scheme 1 and 2 give rise to an amorphous precipitated product that contains roughly 24% water and the amorphous character is maintained during dehydration. After the "so-called" lithiation reactions from Refs. [11, 12] (Figure 3.1), the amorphous phase is maintained for the resulting precipitate. Heating this precipitate to elevated temperature in a reducing atmosphere results in the preparation of crystalline $LiFePO_4$. Unfortunately, the XRD investigation does not provide us with any indication that we are passing through an amorphous $LiFePO_4$ phase. We require the use of different structure characterization tools to investigate these amorphous structures. Mössbauer spectroscopy is perfect for the investigation of the local environment for materials containing Mössbauer active metals such as iron. It has been used in the past to aid in the characterization of $LiFePO_4$ and is ideal for investigating amorphous structures as it depends solely on the local Fe environment [15, 16, 17]. It can clearly identify the oxidation state of the Fe atoms within the structure and is a great tool to fully characterize the two reaction schemes described in Figure 3.1.

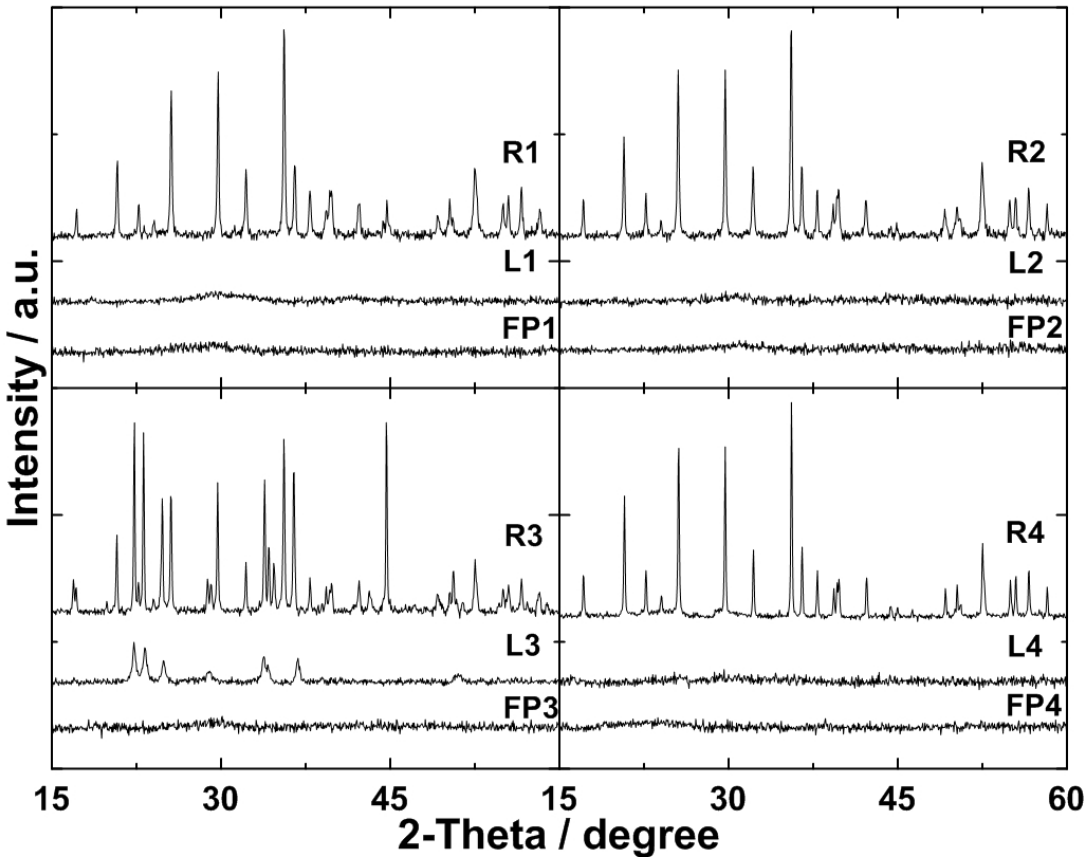

Figure 3.3*: XRD patterns of the precipitated $FePO_4$ (FP1 and FP3) which was dehydrated (FP2 and FP4) followed by a lithiation (L1 through L4) and a thermal treatment (R1 through R4). The symbols used to describe the various products obtained from the reaction schemes are described in Figure 3.1.*

Figure 3.4 provides the Mössbauer spectras for all the prepared samples and their hyperfine parameters are reported in Table 1. In the case of FP1, the sample demonstrates an isomer shift (IS) of 0.41 mm s^{-1} along with a quadrupole splitting (QS) of 0.68 mm s^{-1}. which can be attributed to a purely Fe^{3+} species. This sample after the lithiation reaction, L1, consists of two overlapping doublets. One doublet has an IS of 1.20 mm s^{-1} and a QS of 2.19 mm s^{-1} with an

area of 25% comparing to the second doublet having an IS of 0.38 mm s^{-1}, QS of 0.83 mm s^{-1} which has an area of 75%. The former (IS = 1.20 mm s^{-1}) may be attributed to a Fe^{2+} species and the later (IS = 0.38 mm s^{-1}) to a Fe^{3+} species [17]. The product of the thermal treatment, R1, has two doublets. The first doublet has an area of 96% with an IS of 1.21 mm s^{-1} and a QS of 2.96 mm s^{-1} which corresponds to an octahedral Fe^{2+} species with high spin 3d electrons which is typically obtained for $LiFePO_4$ [17, 18]. The second one has an IS of 0.35 mm s^{-1} and a QS of 0.78 mm s^{-1} with an area of 4%, which corresponds to a small amount of Fe^{3+} containing impurity which is possibly amorphous since it is not clearly visible on the XRD pattern (Figure 3.3). These data suggest that the lithiation step did not give rise to amorphous $LiFePO_4$ since the Mössbauer spectrum shows that the lithiation product has only a minor amount of Fe^{2+} ions. A thermal treatment step is necessary for the formation of $LiFePO_4$. This suggests that a lithium containing salt was present on the surface of the amorphous $FePO_4$ during heating which ultimately reacted to give crystalline $LiFePO_4$. A more detailed analysis of the Mössbauer spectra, shows very sharp peaks for the product R1, which suggests a well structured crystalline material, while FP1 and L1 contain broad/diffuse doublets that are characteristic of amorphous materials [19]. These results are supported by the XRD investigation shown in Figure 3.3.

***Table 3.1**: Hyperfine parameters for the products at each step of S1 and S2*

Sample	IS ($mm\ s^{-1}$)	QS ($mm\ s^{-1}$)	Γ ($mm\ s^{-1}$)	Relative area (%)
FP1	0,41	0,68	0,16	100
L1	0,38	0,83	0,15	75
	1,20	2,19	0,15	25
R1	1,21	2,96	0,14	96
	0,35	0,78	0,14	4
FP2	0,38	0,94	0,38	100
L2	0,40	0,84	0,40	52
	1,15	2,31	0,40	48
R2	1,22	2,98	0,14	94
	0,39	0,89	0,14	6
FP3	0,41	0,73	0,40	100
L3	0,40	0,71	0,33	100
R3	1,23	2,97	0,19	72
	0,01[a]	0,00	0,19	28
FP4	0,37	0,91	0,40	100
L4	1,14	2,37	0,60	56
	0,41	0,79	0,60	44
R4	1,22	2,97	0,16	100

a) Data corresponds to metallic iron with a magnetic hyperfine field of 33.0 T

In the case of the reaction involving dehydrated $FePO_4$, FP2, we obtain a doublet with a measured IS and QS of 0.38 and 0.94 mm s^{-1} respectively. This suggests a presence of purely Fe^{3+} species. The product of the lithiation step, L2, contains Fe^{3+} species with IS of 0.40 and QS of 0.84 mm s^{-1} and a large amount of Fe^{2+} species with an IS of 1.15 and QS of 2.31 mm s^{-1}. The relative area of the Fe^{3+} is 52% while the Fe^{2+} is 48%. These results indicate that for S1, the dehydrated species can be lithiated (reduction of Fe^{3+} to Fe^{2+}) to a larger extent than the hydrated species (Fe^{2+} increases from 25% to 48% after dehydration) but, in both cases, the reaction does not go to completion. There is still a significant amount of Fe^{3+} remaining in the product. When the product of the lithiation reaction, L2, is thermally treated at 600 °C, crystalline $LiFePO_4$, R2, is obtained. The Mössbauer spectra of R2 demonstrates Fe^{2+} species with IS and QS of 1.22 and 2.98 mm s^{-1} respectively with an area of 94% and a Fe^{3+} impurity species with IS and QS of 0.39 and 0.89 respectively with an area of 6%. As mentioned previously, the thermal treatment is necessary for the complete formation of $LiFePO_4$ and the formation of $LiFePO_4$ is not complete simply after the lithiation reaction. An unreacted lithium salt may be present on the surface of a-$FePO_4$ after the incomplete lithiation reaction along with some organic material. Once the material is heated to 600 °C, $LiFePO_4$ is formed via a solid state reaction between the lithium salt, carbon material and a-$FePO_4$. Thus, although we are able to obtain some reduction and the production of some Fe^{2+} species that are amorphous in L1 and L2, the reaction is not complete and the product is not pure amorphous $LiFePO_4$. The lack of Mössbauer data (or other methods to investigate electronic states) in previous work causes much doubt in our minds that a pure amorphous $LiFePO_4$ is indeed produced.

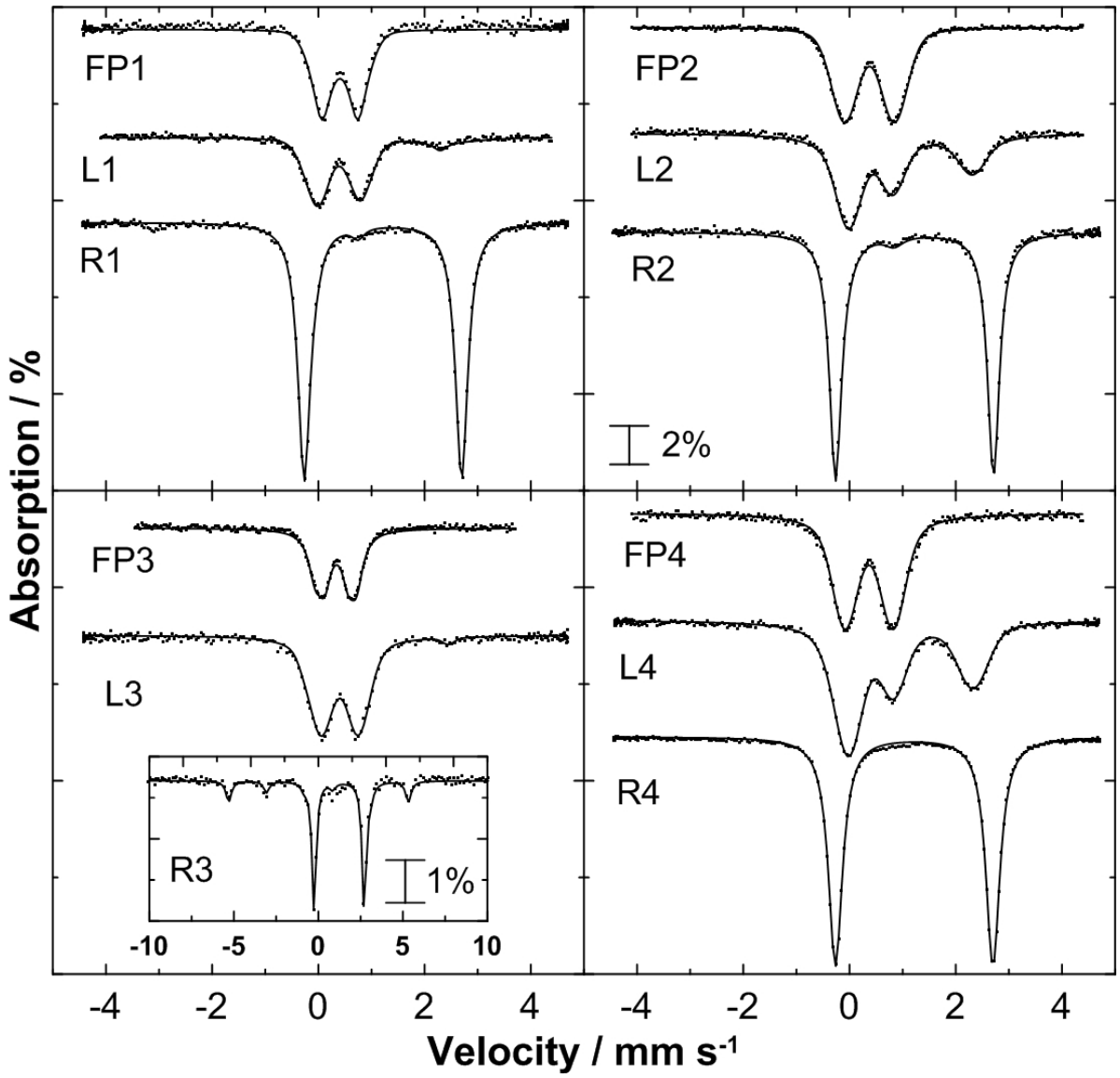

Figure 3.4: *Mössbauer spectra of all the synthesized samples from Figure 3.1. For R3, the scanning parameters were modified in order to detect minor Fe impurities.*

The a-$FePO_4.xH_2O$ (FP3) that was synthesized with the second synthesis route (S2) demonstrates an IS of 0.41 mm s^{-1} and a QS of 0.73 mm s^{-1} which corresponds to an Fe^{3+} species with an area of 100%. Following the lithiation reaction, (L3) the sample has only one doublet

with IS of 0.40 mm s^{-1} and QS of 0.71 mm s^{-1} suggesting a purely Fe^{3+} species. Once the thermal treatment is performed on L3, R3 is obtained. The data suggest the presence of a Fe^{2+} species with an area of 72% along with IS of 1.23 mm s^{-1} and a QS of 2.97 mm s^{-1} which is in the normal range for $LiFePO_4$. The remaining 28% of the spectral area is in the form of a magnetic sextet and reflects the presence of metallic iron which is confirmed with XRD by the presence of an intense peak at approximately 45° [20].

The dehydrated $FePO_4$ from the second synthesis route (FP4) has an IS of 0.37 mm s^{-1} and a QS of 0.91 mm s^{-1} with a relative area of a 100% suggesting a pure Fe^{+3} species. Once the lithiation reaction is performed with LiI in acetonitrile, the obtained sample (L4) has two doublets. The first doublet has an IS of 0.41 mm s^{-1} and a QS of 0.79 mm s^{-1} and the second one has an IS of 1.14 mm s^{-1} and a QS of 2.37 mm s^{-1} with relatives area of 44% and 56% respectively. This former doublet can be attributed to a Fe^{3+} species and the later to a Fe^{2+} species. When the thermal treatment is performed at 600 °C under Ar/H_2, R4 is obtained which contains only an Fe^{2+} species with IS and QS of 1.22 mm s^{-1} and 2.97 mm s^{-1}. The hyperfine parameters of R4 are typical of those obtained for $LiFePO_4$ which is in agreement with the XRD patters (Figure 3.3). Clearly for LiI in acetonitrile, the lithiation of a-$FePO_4$ is improved in the case of the dehydrated sample as compared to the hydrated sample. The dehydrated samples (L2 and L4) are lithiated (reduced) to a larger extent, possibly due to an easier accessibility of the active site by the reductant as opposed to the hydrated samples (L1 and L3) which contain a fair amount of structural water. Nevertheless, full lithiation is not achieved. A pure Fe^{2+} species is only obtained after thermal treatment suggesting that pure amorphous $LiFePO_4$ is not obtained.

A detailed analysis of the Mössbauer data for the lithiated samples (L1 through L4) provides information on the various coordination for Fe in the samples. The data for all Fe^{2+} species in the lithiated samples have IS values higher than 1.14 mm s^{-1}. Typically, values of IS below 1 mm s^{-1} signify a tetrahedral coordination around the Fe atom and IS values above 1 mm s^{-1} signify an octahedral coordination [17]. This suggests that the Fe^{2+} present in the lithiated samples are in an octahedral bonding environment. It is important to note that, even with an octahedral coordination, it cannot be confirmed that the material is an olivine structure due to the amorphous nature of the lithiated intermediates.

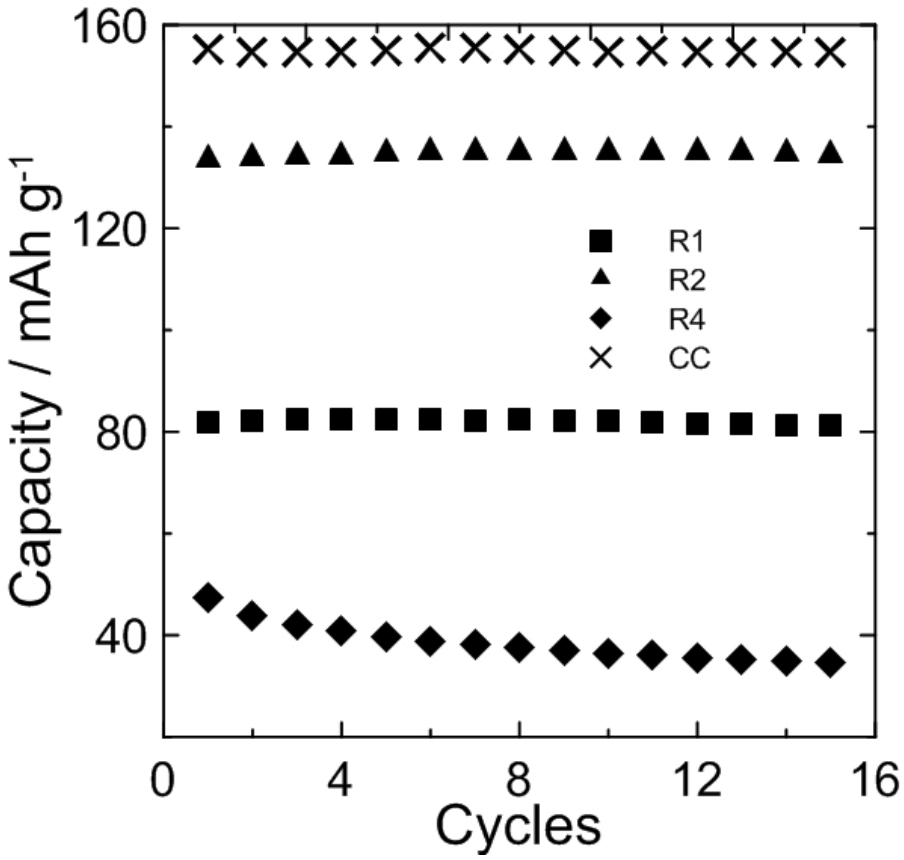

Figure 3.5: *Electrochemical performance of the synthesized $LiFePO_4$ material*

The electrochemical performance of the crystalline $LiFePO_4$ samples (R1-R4) is displayed in Figure 3.5. In the case of R1, the initial discharge capacity is 82 $mAhg^{-1}$. No capacity fade is observed during the experiment. For R2, the first discharge capacity is 128 $mAhg^{-1}$ and similarly to R1, the capacity is stable. The performance is poor when compared to the theoretical capacity of $LiFePO_4$ (170 $mAhg^{-1}$). The low capacity is due to the low carbon content and inefficient carbon coating for these samples. The samples typically contain just 1% carbon which is significantly lower than that required for optimal electrochemical performance [21]. When either R1 or R2 is carbon coated (CC on Figure 3.5) by dissolving 10% B-lactose in a solution of R1 or R2, followed by drying and thermal treatment at 700 °C under N_2, the samples display a significant improvement in performance yielding up to 92% of the theoretical capacity. In the case of R3, values below 10 $mAhg^{-1}$ were observed (not displayed in Figure 3.5) due to high levels of impurities, mainly Li_3PO_4. For R4, the low capacity obtained is due to the extended annealing time at elevated temperature which results in increased particle size and can be associated with a decrease in performance.

3.4 Conclusion

Two different synthetic routes to prepare $LiFePO_4$ which involved the precipitation, chemical lithiation and thermal treatment of an amorphous $FePO_4$ sample were reproduced. The product of each step of the synthesis was characterized using XRD and Mössbauer spectroscopy. We have observed that for both synthetic routes, a dehydrated $FePO_4$ precursor can be lithiated in solution to a greater extent than a hydrated $FePO_4$ precursor. Nevertheless, the iron species after chemical lithiation are composed of both Fe^{3+} and Fe^{2+} indicating that the lithiation step

does not reach completion. Since the initial lithiation reaction is incomplete, a thermal treatment step, which was described in the literature as only associated with crystallization, is essential for the formation of and reduction to $LiFePO_4$. This reaction relies on lithium ions or salts present on the surface of the amorphous $FePO_4$ after lithiation. This is confirmed by Mössbauer data before (where the majority of Fe is Fe^{3+}) and following the heating step (most of the Fe ions are Fe^{2+} in nature) where the hyperfine parameters are typical of an olivine $LiFePO_4$ material. This is confirmed via XRD that demonstrates the clear presence of crystalline $LiFePO_4$ after thermal treatment that was also found to be electrochemically active. The authors would like to stress the importance of Mössbauer spectroscopy in evaluating the reaction mechanism of these reactions and note its critical importance in investigating the characteristic of the amorphous precursors.

Acknowledgements

The authors thank NSERC and Phostech Lithium for funding this work under the auspices of the Industrial Research Chair program.

3.5 References

1. Chen, Z.; Dahn, J. R., *J. Electrochem. Soc.*, **2002**, 149, 1184.
2. Zhang, S. S.; Allen, J. L.; Xu, K.; Jow, T. R., *J. Power Sources* **2005**, 147, 234.
3. Higuchi, M.; Katayama, K.; Azuma, Y.; Yukawa, M.; Suhara, M., *J. Power Sources*, **2003**, 119, 258.
4. Dokko, K.; Koizumi, S.; Sharaishi, K., *J. Power Sources*, **2007**, 165, 656.
5. Meligrana, G.; Gerbaldi, C.; Tuel, A.; Bodoardo, S.; Penazzi, N., *J. Power Sources*, **2006**, 160, 516.
6. Park, K. S.; Son, J. T.; Chung, H. T.; Kim, S. J.; Lee, C. H.; Kim, H. G., *Electrochem. Commun.*, **2003**, 5, 839.
7. Kim, J.-K.; Cheruvally, G.; Choi, J.-W.; Kim, J.-U.; Ahn, J.-H.; Cho, G.-B.; Kim, K.-W.; Ahn, H.-J., *J. Power Sources*, **2007**, 166, 211.
8. Zhu, B.Q.; Li, X.H.; Wang, Z.X.; Guo, H.J., *Mater. Chem. Phys.*, **2006**, 98, 373.
9. Andersson, A.S.; Thomas, J.O.; Kalska, B.; Haggstrom, L., *Electrochem. Solid State Lett.*, **2000**, 3, 66.
10. Chung, S.-Y.; Bloking, J. T.; Chiang, Y.-M., *Nat. Mater.*, **2002**, 1, 123.
11. Wang, B.; Qiu, Y.; Ni, S., *Solid State Ionics*, **2007**,178, 843.
12. Prosini, P.P.; Carewska, M.; Scaccia, S.; Wisniewski, P.; Passerini, S.; Pasquali, M., *J. Electrochem. Soc.*, **2002**, 149, 886.
13. Zaghib, K.; Ait Salah, A.; Ravet, N.; Mauger, A.; Gendron, F.; Julien, C. M., *J. Power Sources*, **2006**,160, 1381.
14. Scaccia, S.; Carewska, M.; Wisniewski, P.; Prosini, P. P., *Mat. Res. Bul.*, **2003**, 38, 1155.

15. Sanchez, M. A. E.; Brito, G. E. S.; Fantini, M. C. A.; Goya, G. F.; Matos, J.R., *Solid State Ionics*, **2006**, 177, 497.

16. Kim, C. W.; Lee, M. H.; Jeong, W. T.; Lee, K. S., *J. Power Sources*, **2005**, 146, 534.

17. Hirose, K.; Honma, T.; Doi, Y.; Hinatsu, Y.; Komatsu, T., *Solid State Commun.*, **2008**, 146, 273.

18. Prince, A. A. M.; Mylswamy, S.; Chan, T. S.; Liu, R. S.; Hannoyer, B.; Jean, M.; Shen, C. H.; Huang, S. M.; Lee, J. F.; Wang, G. X., *Solid State Commun.*, **2004**, 132, 455.

19. Yu, X.; Day, D. E.; Long, G. J.; Brow, R. K., *J. Non-Cryst. Solids*, **1997**, 215, 21.

20. Kim, K. H.; Lee, J. D.; Lee, J. J.; Ahn, B. Y.; Kim, H. S.; Shin, Y. W., *Thin Solid Films*, **2005**, 483, 74.

21. Cho, Y.-D.; Fey, G. T.-K.; Kao, H.-M., *J. Power Sources*, **2009**, 189, 256.

Chapter 4

Cost effective synthesis of Li_2FeSiO_4

4.1 Introduction

Rechargeable Li-ion batteries are becoming increasingly important in portable electronic application as well as electrical vehicles. The advantage of this technology is the high energy density that can be obtained. On the other hand, rechargeable Li-ion batteries are expensive to manufacture with costly components such as electrolyte, separators and electrode materials. A large amount of research is devoted to finding optimum materials that could be both cost effective and have high energy density. In this chapter, a novel synthesis of Li_2FeSiO_4 will be presented. The motivation behind this research is to obtain Li_2FeSiO_4 starting with low cost precursors and simple laboratory equipment in order to reduce the overall synthetic cost of this electrode material.

As mentioned previously in Chapter 1, Li_2FeSiO_4 was first synthesized and characterized by Nyten et al in 2005 [1]. Since then, many different synthetic routes have been employed to obtain the material such as citric-assisted sol-gel method [2], solid-state method [3, 4] and hydrothermal method [5]. In this study, a solid-state method was chosen and low cost precursors were selected (Li_2CO_3, Fe_2O_3 and SiO_2). Beta-lactose (β-lactose) was chosen as the reducing agent although other forms of carbon precursor would likely work just as well.

4.2 Results and Discussion

The reaction to synthesize Li_2FeSiO_4 was selected based on inexpensive precursors and can be described as:

$$Li_2CO_3 + \frac{1}{2}Fe_2O_3 + SiO_2 + (x)\ C_{12}H_{22}O_{11} \rightarrow Li_2FeSiO_4 + (y)\ CO_2 + (z)\ H_2O.$$

This reaction scheme gave rise to the desired material along with some side products of various gases. The temperature of the synthesis and the amount of the carbon precursor (β-lactose) was varied to optimize the procedure. The β-lactose content was based on the theoretical amount of Li_2FeSiO_4 to be formed which was 3.5 grams; hence when referred to a sample containing 10 wt% of β-lactose that would imply that 0.35 grams of β-lactose was added to the precursor mixture. Initially, the milled precursors containing 16 wt% of β-lactose were heated to temperatures ranging from 650 to 900 °C for 3 hours under N_2 atmosphere. The XRD diffraction patterns are demonstrated in Figure 4.1. At 800 °C, pure Li_2FeSiO_4 is formed giving rise to a diffraction profile similar to what is obtained in the literature [1-5]. At 850 °C and 900 °C, Li_2FeSiO_4 is formed as well but the powder tends to adhere to the porcelain crucible leading to a lower product yield. The synthesized Li_2FeSiO_4 was light gray in color. At 700 and 750 °C, some Li_2FeSiO_4 is formed but the samples contain significant amount of Li_2SiO_3. At 650 °C, a large amount of Li_2SiO_3 is present with no peaks indicating the presence of Li_2FeSiO_4. Thus, the temperature for further investigation was chosen to be 800 °C.

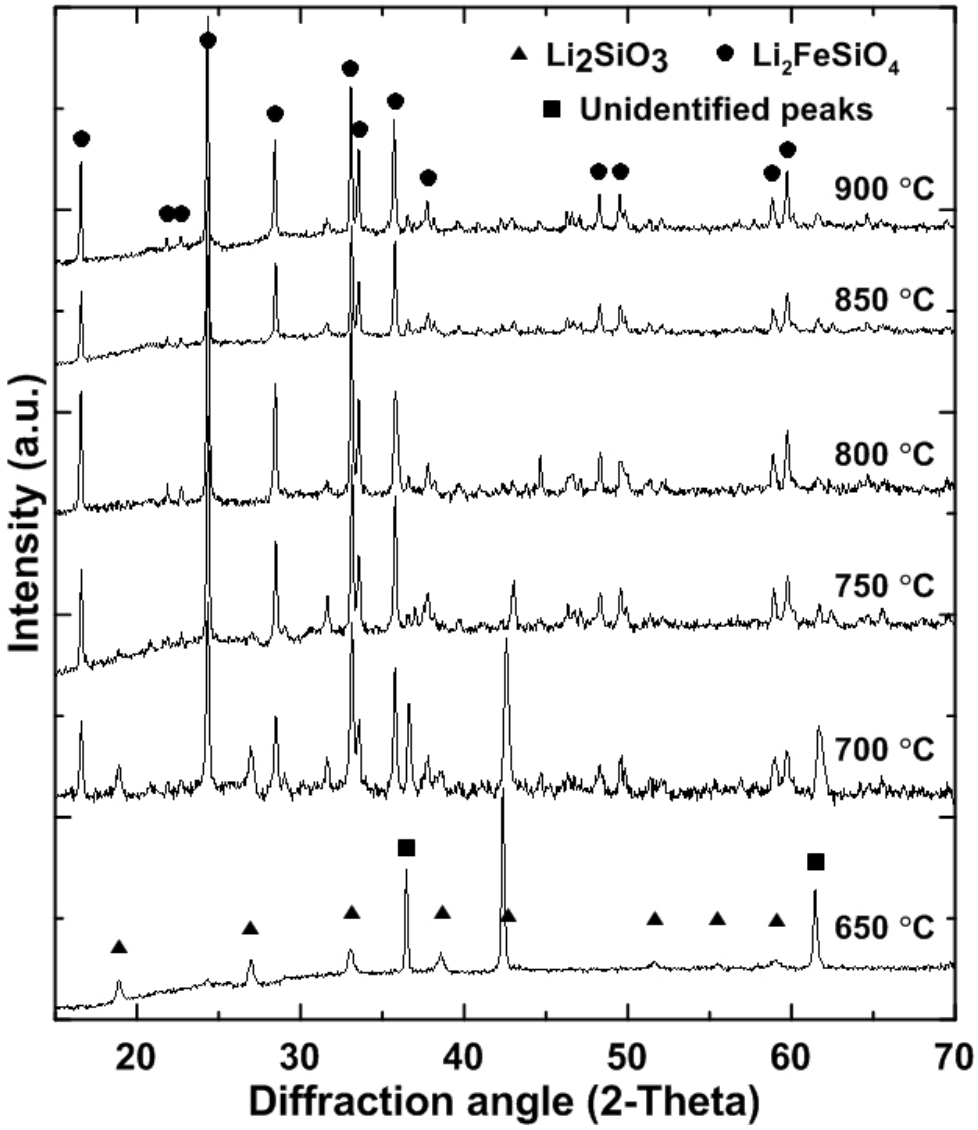

Figure 4.1*: XRD patterns of the samples containing 16 wt% β-lactose, heated to temperatures ranging from 650 to 900 °C*

The next step was to determine the optimum β-lactose content for the synthesis in order to avoid side reactions. The precursors were mixed with various amount of β-lactose ranging from 4 to 16 wt% and then heated to 800 °C. The XRD patterns are demonstrated in Figure 4.2. Samples that contained 6 wt% or more β-lactose in the mixture result in what seems to be almost

pure Li_2FeSiO_4. For the sample containing 4 wt% β-lactose, a large amount of Li_2SiO_3 is obtained due to insufficient quantity of β-lactose which acts as a reductant. At 16 wt% β-lactose, a peak at approximately 44.5° indicates of α-Fe suggesting that under these reductive conditions too much carbon is present which leads to the reduction of Fe^{2+} to Fe metal [6].

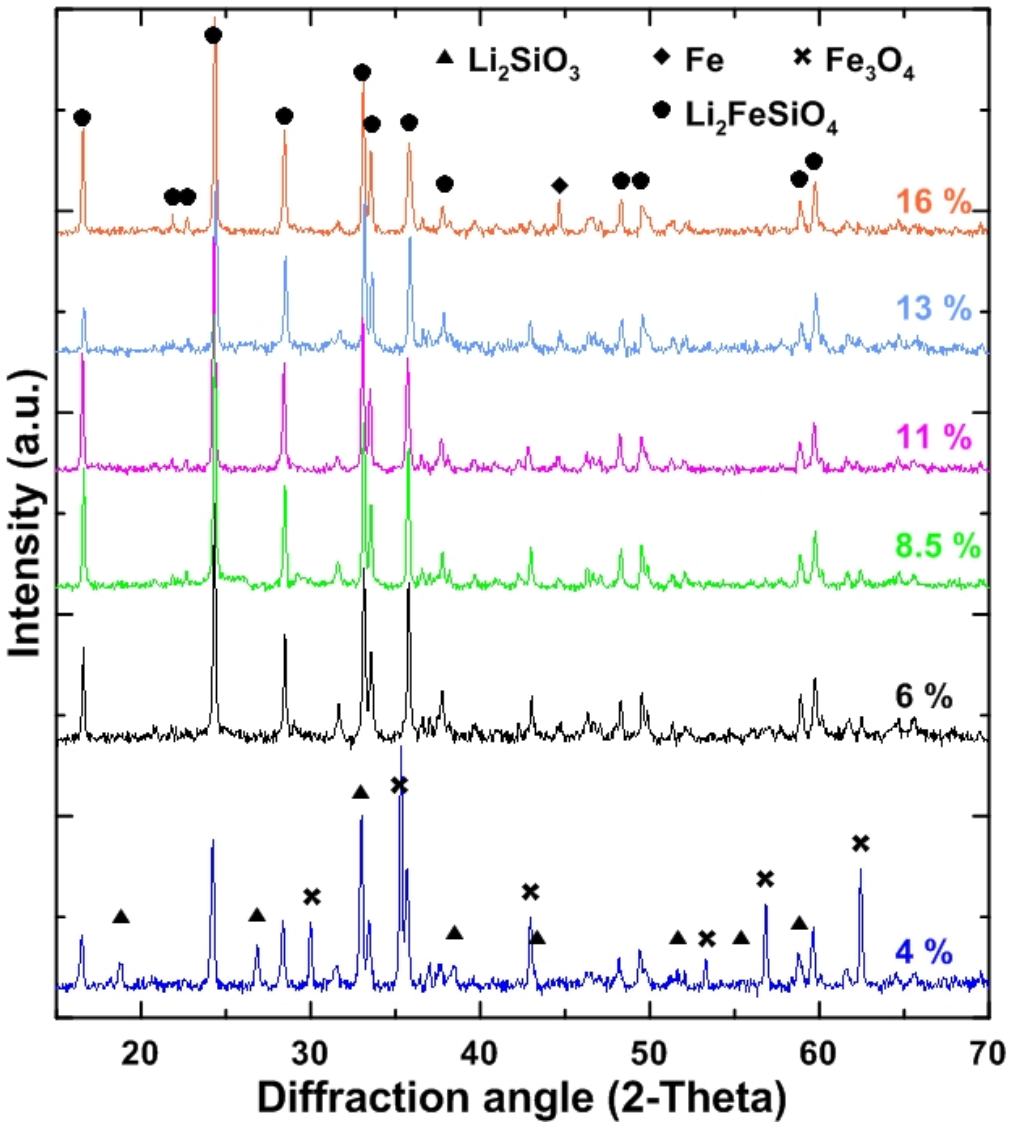

Figure 4.2*: XRD diffraction patterns of the thermally treated samples at 800 °C with a β-lactose content varying from 4 to 16 wt%.*

The particle size and the morphology of the synthesized samples were analyzed using SEM. Figure 4.3 shows the SEM images of a sample containing 13% wt β-lactose in the precursor mixture heated to 800 °C for 3 hours. The sample consists of non-uniform agglomerates typically 3 to 7 μm in size (Figure 4.3A). The agglomerates are formed from smaller interconnected particles ranging from 300 nm up to 1 μm (Figure 4.3B). Traditionally, Li_2FeSiO_4 with a smaller particle size, in the range of 50 to 250 nm is favored due to shorter diffusions path for the lithium atom within the particle leading to an overall increase in performance [7, 8]. The solid-state synthesis used here leads to large particle size material due to an extended exposure of the sample to elevated temperatures which leads to an annealing process. Hence, a milling procedure was performed on the obtained material to reduce the particle size. This should result in superior performance [9].

After the synthesis, the carbon content for the obtained samples, from varying initial ß-lactose amount, was measured. The measurements were performed at the "Laboratoire d'analyse élémentaire" at Université de Montréal. Table 4.1 demonstrates the wt% of β-lactose before the synthesis and the wt% of carbon measured following the thermal treatment at 800 °C. The precursor mixtures that contained 4 and 6 wt% of β-lactose have a carbon content of 0.12 and 0.10 wt% respectively. These values were at the limit of detection of the analytical characterization method. For this synthesis, residual carbon is not desired due to the possibility to reduce iron further from the desired Fe^{2+} during the thermal treatment, therefore the amount of carbon precursor needs to be precisely controlled. In this case, the optimal amount of β-lactose was determined to be 8.5 wt%, this gave rise to a residual carbon content of 0.36 wt%. The

sample which contained 6 wt% of β-lactose was not optimal due to low excess carbon leading to the possible presence of amorphous unreacted impurities which would not be visible by XRD.

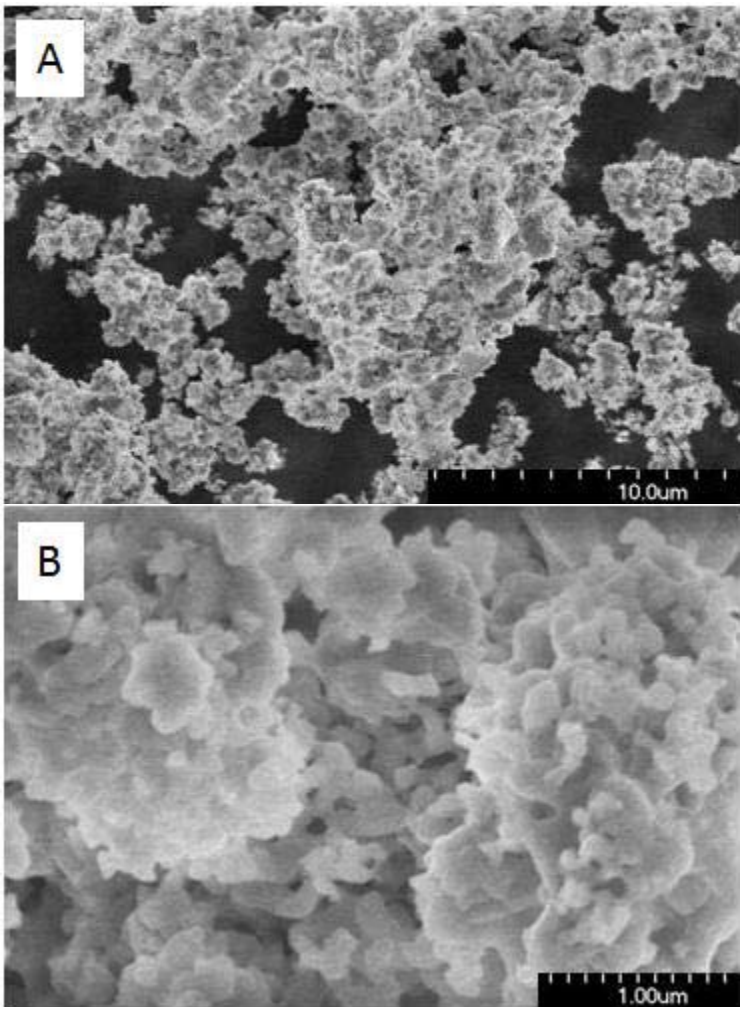

Figure 4.3*: SEM data at different magnification (A with a scale bar of 10 µm and B with a scale bar of 1µm) for the synthesized Li_2FeSiO_4 containing 13 wt% β-lactose in the precursor mixture*

***Table 4.1**: β-lactose content added to the mixture along with the carbon content of the resulting sample after thermal treatment at 800 °C for 3 hours*

β-lactose (wt%)	Carbon (wt %)
13	0.54
11	0.56
8.5	0.36
6	0.10*
4	0.12*

*The signal is at the detection limit of the analysis method

TGA and DSC data were obtained for the prepared Li_2FeSiO_4 resulting in 0.36 wt% carbon in the synthesized product. The data is presented in Figure 4.4. The sample was initially flushed with He gas and then heated to 1300 °C with a heating rate of 20 °C per minute. The weight loss and heat flow were recorded during the heating step as well as the cooling step. Although the cooling step was set to 20 °C per minute, the apparatus does not contain a rapid cooling system so there are likely deviations from the set rate. The TGA curve is shown in red, while the associated DSC curve is shown in blue. From the beginning of the experiment up to about 800 °C, a weight loss of approximately 8.5% is obtained. From the simultaneous Mass Spectroscopy analysis of the gas, the 8.5% weight change is due to the loss of CO_2. The weight of the sample after 800 °C then stays constant up to approximately 1230 °C where small spike is then observed. During the cooling of the sample, the weight does not change. In the case of the DSC, during the heating step a small exothermic event is observed at approximately 975 °C which has not been identified. There is also an endothermic event at 1234 °C which is associated to the melting of the sample. During the cooling step, a large exothermic event is observed at

1164 °C which can be associated with the crystallization of Li_2FeSiO_4. Also, four small exothermic events are observed between approximately 1100 °C and 850 °C which have not yet been identified.

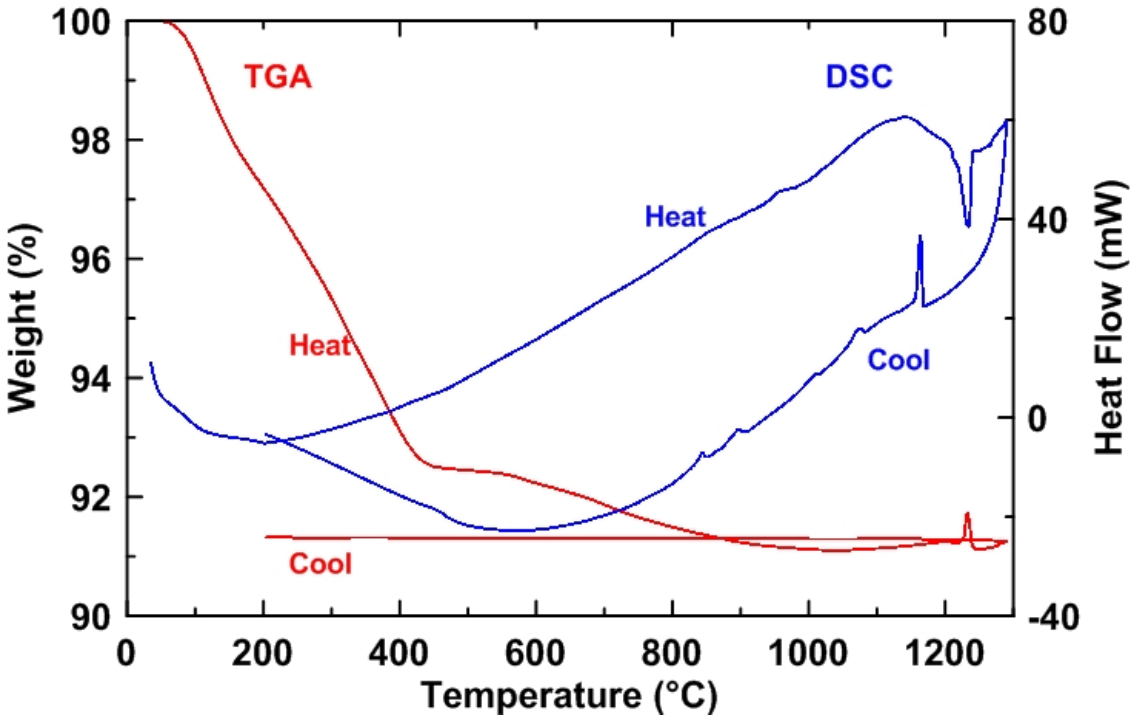

***Figure 4.4**: TGA and DSC curves for the synthesized Li_2FeSiO_4*

The synthesized Li_2FeSiO_4 with 8.5 wt% β-lactose in the precursor mixture was then milled in order to reduce the particle size of the material. Approximately 1.75 grams of Li_2FeSiO_4 was milled in IPA for 90 minutes using a 250 ml Syalon container with 100 grams of Syalon milling media. The powder was passed through a 38 µm sieve in order to remove large aggregates [9]. The final powder was then carbon coated. Due to the low intrinsic conductivity of

Li_2FeSiO_4, a carbon coating step is essential to enhance the electrical conductivity and obtain improved electrochemical performance from the material. The synthesized powder was suspended and stirred in an aqueous solution containing 10 wt% of β-lactose until all the water was evaporated. The resulting powder was then thermally treated at 600 °C under N_2 atmosphere for 1 hour. The resulting black carbon coated Li_2FeSiO_4 contained approximately 2.79 wt% carbon. The procedures for milling and carbon coating were described in detail in Chapter 2.

Figure 4.5 shows the voltage versus capacity plot of the carbon coated Li_2FeSiO_4. The battery assembly details are described in the experimental section (Chapter 2). The cut off voltages were set at 2 and 4 V while the experiment was performed using a current of 17 mA g^{-1}. On the first charge/discharge cycle, denoted with the black line, the charging capacity was 129 mAh g^{-1} and the discharging capacity was 109 mAh g^{-1}. During the initial charge a plateau is observed at around 3.1 V and the discharge plateau is at approximately 2.7 V. On the second cycle which is denoted in blue, the voltage plateau during charge drops to 2.8 V while the discharge voltage plateau stays fairly constant. Nytén and al. suggested that the voltage drop after the fist cycle is attributed to a phase transition to a more stable structure [1]. After careful observation of the voltage profile during different cycles, it can be noticed that the voltage gap (hysteresis) between charge/discharge tends to decrease from the 2^{nd} cycle to the 30^{th}. This improvement, reduction of the voltage gap, can be attributed to a stabilization of the two phase region as well as decrease in polarization due to already established channels for lithium and electron mobility [3].

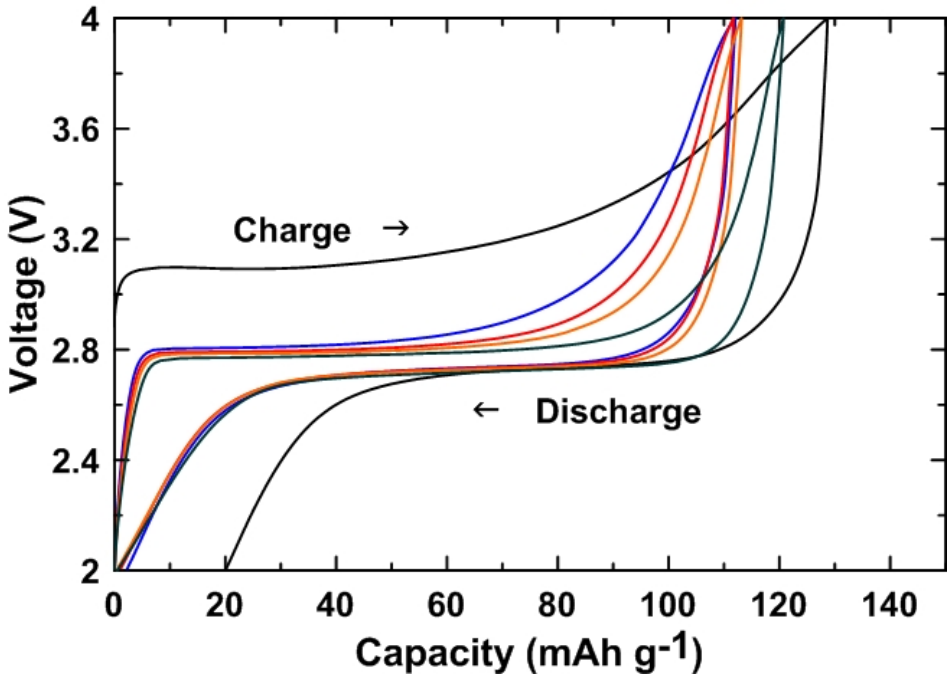

***Figure 4.5**: Voltage versus capacity data of the carbon coated Li_2FeSiO_4. Black, blue, red, orange and green curves correspond to the 1st, 2nd, 5th, 10th and 30th cycles respectively.*

Cycling data is presented in Figure 4.6. The filled dots represent the charge capacity, while the open dots represent the discharge capacity. The cell was cycles for 31 cycles and the discharge capacity increases from 109 mAh g^{-1} on the first cycle to approximately 120 mAh g^{-1} giving rise to 73% of the theoretical capacity (166 mAh g^{-1}) for Li_2FeSiO_4. The first cycle has a poor discharge/charge capacity ratio but this is improved on cycling, suggesting an almost fully reversible reaction.

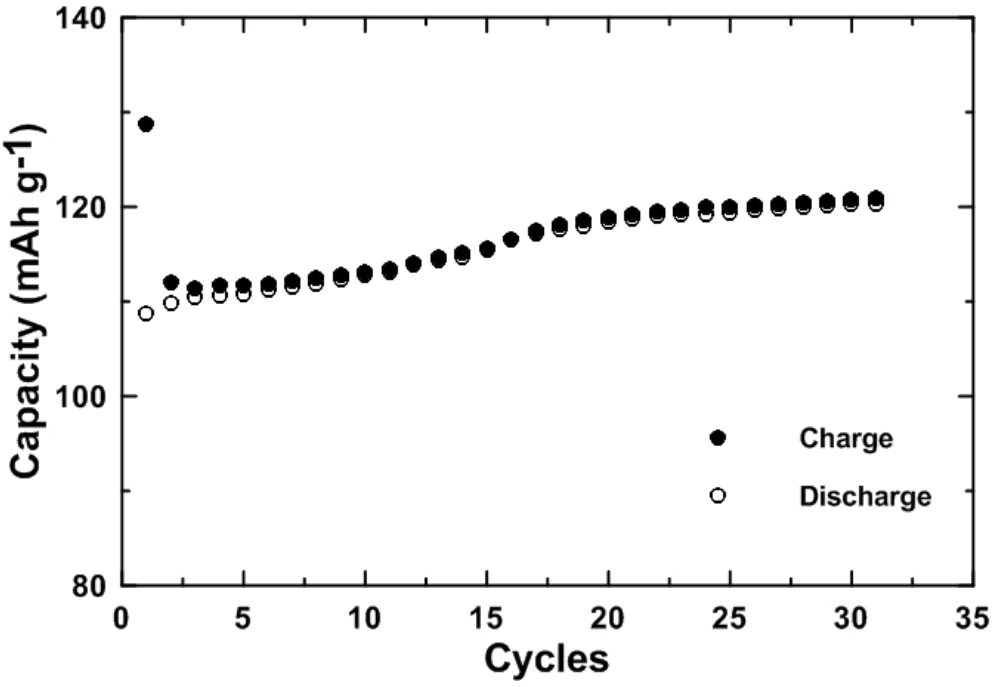

***Figure 4.6**: Charge capacity (filled dots) and discharge capacity (empty dots) versus cycling of the carbon coated Li_2FeSiO_4*

4.3 Attempt to synthesize $Li_{2-2x}Fe_{1+x}SiO_4$ with x = 0.125 and 0.25

As shown previously in section 4.1, Li_2FeSiO_4 obtained from a solid-state synthesis gives rise to ~120 mAh g^{-1} at a current density of 17 mA g^{-1}, extracting only 73% of its the theoretical capacity. Although optimizing the procedure in order to extract higher capacity would be an interesting direction for future work in this case a different approach was taken in order to improve the performance of the material. An attempt was made to synthesize $Li_{1.75}Fe_{1.125}SiO_4$ and $Li_{1.5}Fe_{1.25}SiO_4$. The interest in such compounds is the high theoretical capacity which in the case of $Li_{1.75}Fe_{1.125}SiO_4$ and $Li_{1.5}Fe_{1.25}SiO_4$ is 181 and 194 mAh g^{-1} respectively compared to Li_2FeSiO_4 which has a theoretical capacity of 166 mAh g^{-1} (for a 1 electron reaction). The reason

for the increased theoretical capacity is the addition of Fe^{2+} in the structure which allows a larger amount of Li to be removed due to the larger amount of the $Fe^{2+/3+}$ redox couple present in the material. In these samples, for each atom of Fe added, two atoms of Li could be removed such that the overall charge is balanced. Such substitution should be theoretically feasible to a certain extent due to Fe^{2+} being similar in size (0.74 Å) to Li^{+} (0.76 Å) [2]. Throughout the text, the two synthesized samples will be referred to as $Li_{1.75}Fe_{1.125}SiO_4$ and $Li_{1.5}Fe_{1.25}SiO_4$ although it is unclear whether the samples have that specific stoichiometry or not.

For the synthesis of Li_2FeSiO_4 described in section 4.1, the optimal amount of β-lactose was chosen to be 8.5 wt%. In the case of $Li_{1.75}Fe_{1.125}SiO_4$ the iron oxide content in the precursor mixture was increased by 12.5% in comparison with the iron oxide content in the precursor mixture for Li_2FeSiO_4. The amount of β-lactose was increased by 12.5% as well to complete the necessary reduction of Fe^{3+} to Fe^{2+} during synthesis. Similar for $Li_{1.5}Fe_{1.25}SiO_4$, the iron oxide and the β-lactose content was increased by 25% in the precursor mixture. In order to maintain charge neutrality, the lithium carbonate content in the precursor mixture was decreased by 12.5% and 25% for $Li_{1.75}Fe_{1.125}SiO_4$ and $Li_{1.5}Fe_{1.25}SiO_4$, respectively, when compared to the lithium carbonate content in the precursor mixture for Li_2FeSiO_4. The method of synthesis for these off-stoichimetric compounds was similar to Li_2FeSiO_4. The precursors were milled followed by a thermal treatment at 800 °C for 3 hours under N_2 atmosphere.

The synthesized samples were light gray, similar to the previously described Li_2FeSiO_4 samples. The synthesized powders were milled and the XRD diffraction patterns of the samples

are presented in Figure 4.7. Both samples demonstrate much broader peaks than those obtained for Li_2FeSiO_4. The reason for broader peaks is due to $Li_{1.75}Fe_{1.125}SiO_4$ and $Li_{1.5}Fe_{1.25}SiO_4$ being milled before XRD analysis and Li_2FeSiO_4 was analyzed right after the synthesis such that Li_2FeSiO_4 contained much larger agglomerates which resulted in peaks that are less broad and more intense [9]. In terms of peak position, for $Li_{1.75}Fe_{1.125}SiO_4$ has all the same peaks as for Li_2FeSiO_4 and no impurity phases are visible. The XRD diffraction pattern for $Li_{1.5}Fe_{1.25}SiO_4$ resembles strongly the diffraction pattern of Li_2FeSiO_4 except for an impurity phase with peaks at approximately 24.5, 28 and 34°. The impurity phase was latter characterized as Fe_2SiO_4. Such an impurity arises due to a large increase in the iron and a large decrease in lithium content in the precursor mixture which after the thermal treatment produces a lithium poor and iron rich phase which in this case is Fe_2SiO_4.

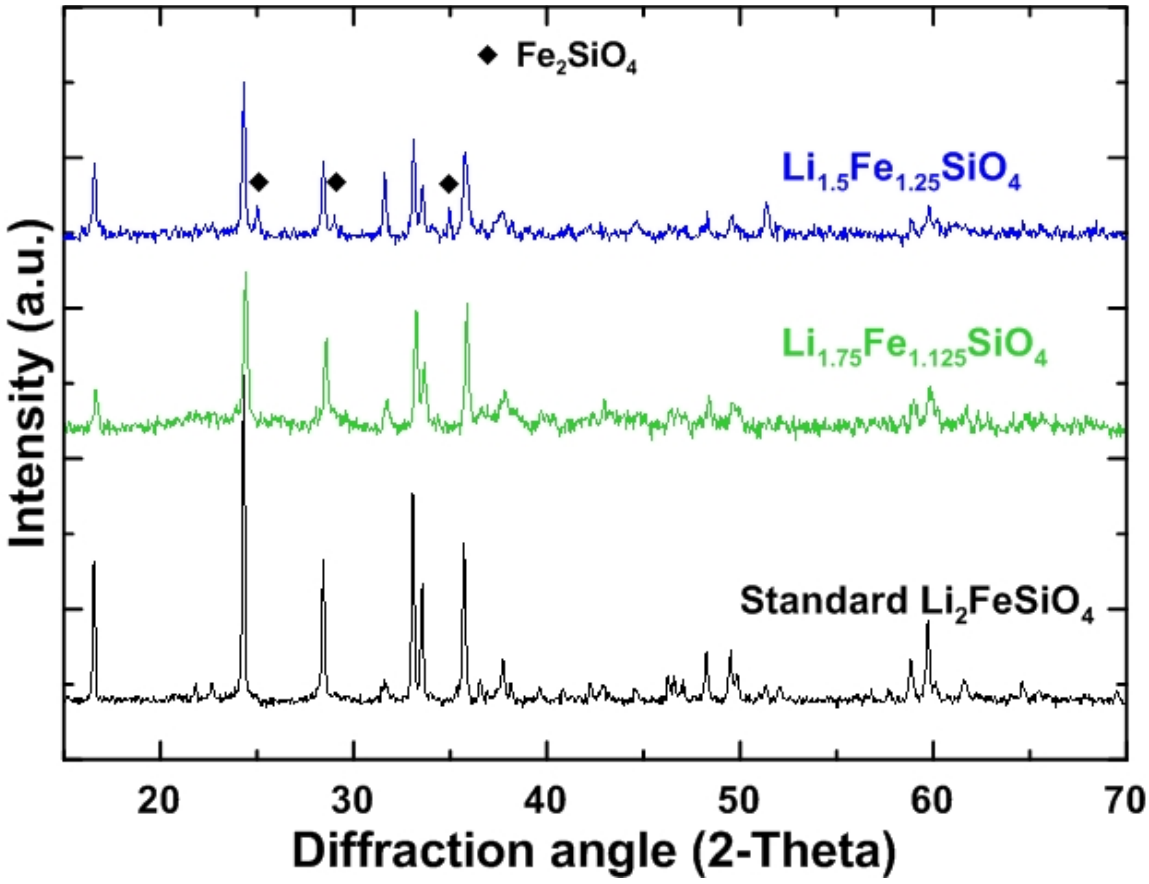

Figure 4.7: *XRD diffractions patterns of the synthesized $Li_{1.75}Fe_{1.125}SiO_4$ and $Li_{1.5}Fe_{1.25}SiO_4$ compared with Li_2FeSiO_4.*

The synthesized samples were analyzed using TGA and DSC under the same conditions as used to analyze Li_2FeSiO_4. The data is presented in Figure 4.8. In both cases, the TGA data suggests little variation in weight with increasing temperature. In the case of $Li_{1.75}Fe_{1.125}SiO_4$ the main endothermic event occurs at 1220 °C which is attributed to the melting of the sample. Two small endothermic events occur at approximately 500 and 875 °C which have not been identified. The main exothermic event occurs on cooling at 1160 °C and is associated with the crystallization process. Four small exothermic events occur during the cooling step between

approximately 900 and 450 °C. The difference between the crystallization and the melting point of Li_2FeSiO_4 and $Li_{1.75}Fe_{1.125}SiO_4$ can be attributed to a small amount of impurities present in $Li_{1.75}Fe_{1.125}SiO_4$ that are not visible from XRD and which lower the samples melting and crystallization point. For $Li_{1.5}Fe_{1.25}SiO_4$ an important endothermic event occurs at 1180 °C which can be attributed to melting of the sample. The event is much broader when compared with the melting of Li_2FeSiO_4 and $Li_{1.75}Fe_{1.125}SiO_4$. This broadness suggests the presence of impurities (Fe_2SiO_4) which was confirmed via XRD. The crystallization point occurs at 1146 °C, a slightly lower temperature than for Li_2FeSiO_4 and $Li_{1.75}Fe_{1.125}SiO_4$. The small endothermic and exothermic events of $Li_{1.5}Fe_{1.25}SiO_4$ are similar to the ones of $Li_{1.75}Fe_{1.125}SiO_4$ except for a small endothermic event occurring at approximately 1000 °C.

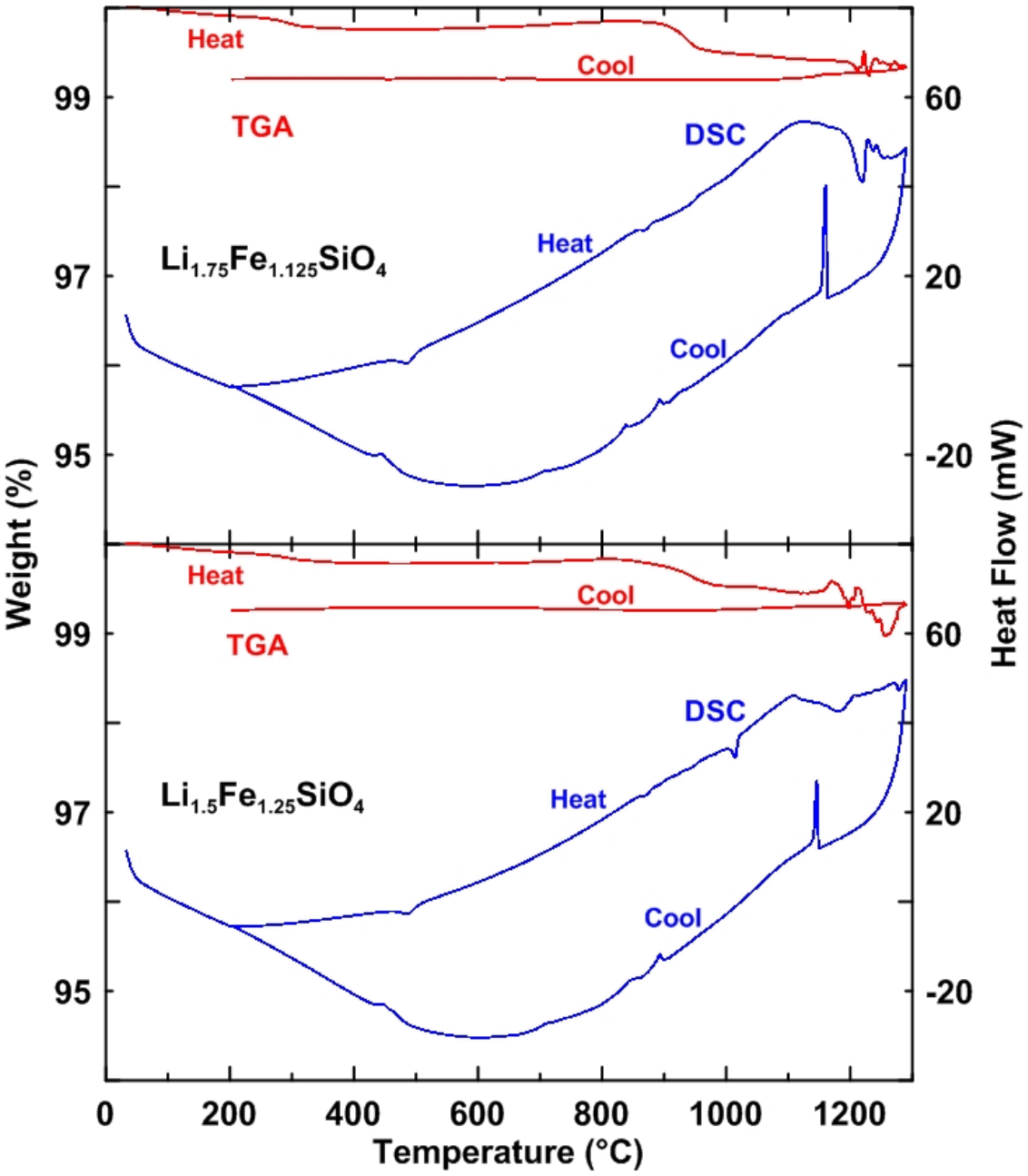

***Figure 4.8**: TGA and DSC for the synthesized $Li_{1.75}Fe_{1.125}SiO_4$ and $Li_{1.5}Fe_{1.25}SiO_4$*

***Table 4.2**: Carbon content of previously synthesized Li_2FeSiO_4 compared to the prepared off-stoichiometric samples*

Sample	Carbon (wt %)
$Li_{1.75}Fe_{1.125}SiO_4$	2.62
$Li_{1.5}Fe_{1.25}SiO_4$	2.74
Li_2FeSiO_4	2.79

The milled samples were carbon coated by the same procedures as for Li_2FeSiO_4 mentioned previously. The carbon content was analyzed and the data is presented in Table 4.2. The carbon content of the synthesized samples, $Li_{1.75}Fe_{1.125}SiO_4$ and $Li_{1.5}Fe_{1.25}SiO_4$, is 2.62 and 2.74 wt%. These values are very close to the carbon content obtained in Li_2FeSiO_4 which is 2.79 wt%.

Coin cells were assembled and the resulting electrochemical data is presented in Figure 4.9 and 4.10 for $Li_{1.75}Fe_{1.125}SiO_4$ and $Li_{1.5}Fe_{1.25}SiO_4$, respectively. For $Li_{1.75}Fe_{1.125}SiO_4$, the first cycle denoted in black demonstrates a charge capacity of 118 mAh g^{-1} and a discharge capacity of 109 mAh g^{-1}. The charging for the first cycle occurs at an approximate voltage of 3.1 V and during discharge a plateau is visible at 2.7 V. During the second cycle, which is denoted in blue, the charging plateau drops to 2.8 V but the discharging plateau stays at 2.7 V which gives rise to 112 mAh g^{-1} during the charge and 111 mAh g^{-1} during discharge. During subsequent cycles, the capacity slowly increased to 117 mAh g^{-1} for the charge cycle and 116 mAh g^{-1} during the discharge cycle. The voltage gap on the 2nd cycle (blue) is slightly larger than on the 10th cycle (orange). This is similar to what was observed for Li_2FeSiO_4 suggesting a good two phase region

and easier access to the active material due to the established channels for lithium and electron migration [3]. The 30th cycle (green) demonstrates no change in the size of hysteresis although it can be noticed that the charge/discharge plateau shifts slightly to lower voltage. Such behavior was not noticed for Li_2FeSiO_4 and at this point is not well understood.

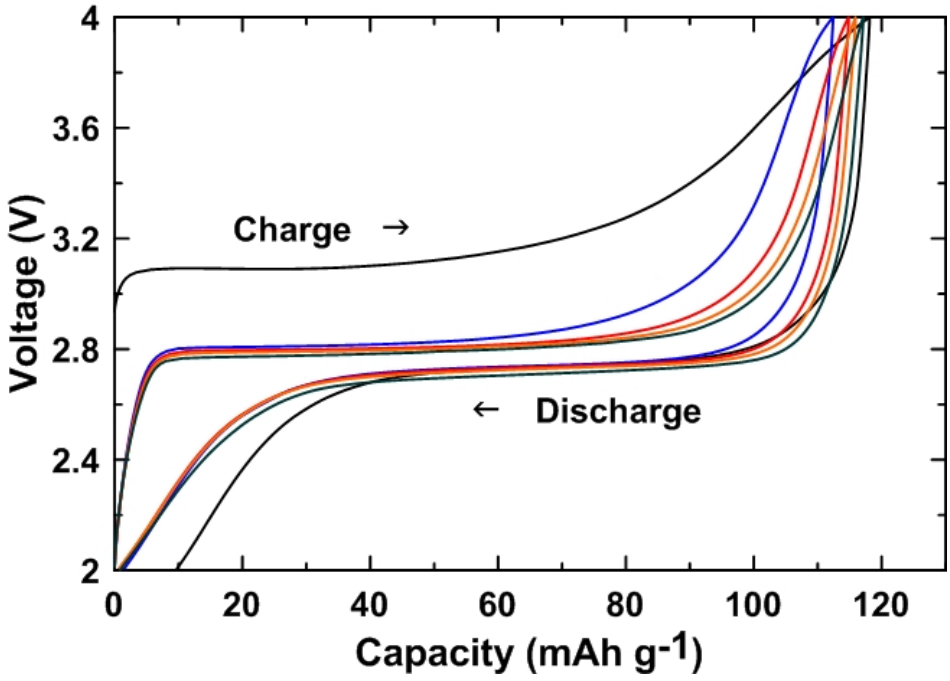

Figure 4.9: *Voltage versus capacity plot of carbon coated $Li_{1.75}Fe_{1.125}SiO_4$. Black, blue, red, orange and green curves correspond to the 1st, 2nd, 5th, 10th and 30th cycles respectively.*

Electrochemical data for $Li_{1.5}Fe_{1.25}SiO_4$ is presented in Figure 4.10. A plateau on the first cycle (black) is visible at 3.1 V for charge and 2.7 V for discharge. The capacity obtained on the first cycle is 81 mAh g^{-1} for charge and 73 mAh g^{-1} for discharge. On the second cycle (blue), the charging voltage plateau drops to 2.8 V and the discharging plateau stays constant. The voltage

gap between the charge/discharge plateaus tends to get smaller from the 1st cycle to the 5th. On the 10th cycle the gap becomes slightly larger and it is further expanded on the 30th cycle. It can be noticed that the gap between the two plateaus is getting larger due to the discharge plateau occurring at a lower voltage for the 10th and 30th cycle (orange and green respectively). The charge plateau is slightly lower in voltage from the 2nd to the 30th cycle but much less when compared to the discharge plateau.

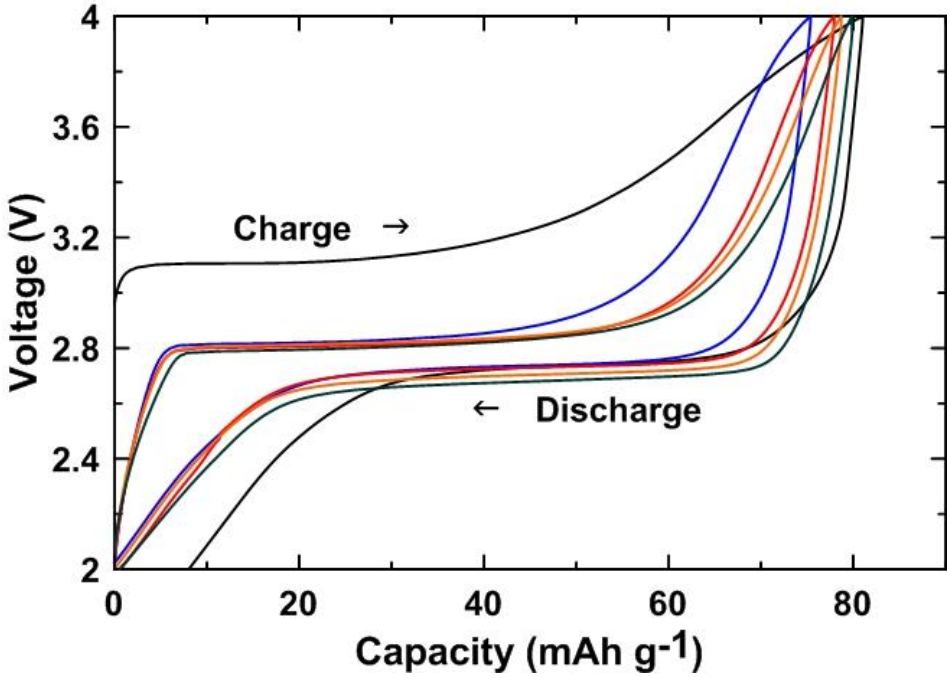

Figure 4.10: *Voltage versus capacity plot of carbon coated $Li_{1.5}Fe_{1.25}SiO_4$. Black, blue, red, orange and green curves correspond to the 1st, 2nd, 5th, 10th and 30th cycles respectively.*

Cycling data for carbon coated $Li_{1.75}Fe_{1.125}SiO_4$ and $Li_{1.5}Fe_{1.25}FeSiO_4$ is presented in Figure 4.11. In the case of $Li_{1.75}Fe_{1.125}SiO_4$, denoted by black filled triangles for charge and open

triangles for discharge, the sample demonstrates stable capacity over 31 cycles. Towards the last cycles, the discharge capacity is 117 mAh g^{-1} and the charge capacity is 116 mAh g^{-1} suggesting an almost complete reversible reaction. For $Li_{1.5}Fe_{1.25}SiO_4$, denoted by black circles for charge and white circles for discharge, the capacity stabilizes at 80 and 79 mAh g^{-1} for charge and discharge respectively. The material is stable over 31 cycles with an almost reversible reaction. When comparing the discharge capacity numbers obtained for the synthesized samples with Li_2FeSiO_4, it is clear that $Li_{1.5}Fe_{1.25}SiO_4$ gives lower performance, 79 mAh g^{-1}, and $Li_{1.75}Fe_{1.125}SiO_4$ and Li_2FeSiO_4 are almost identical at 117 and 120 mAh g^{-1} respectively.

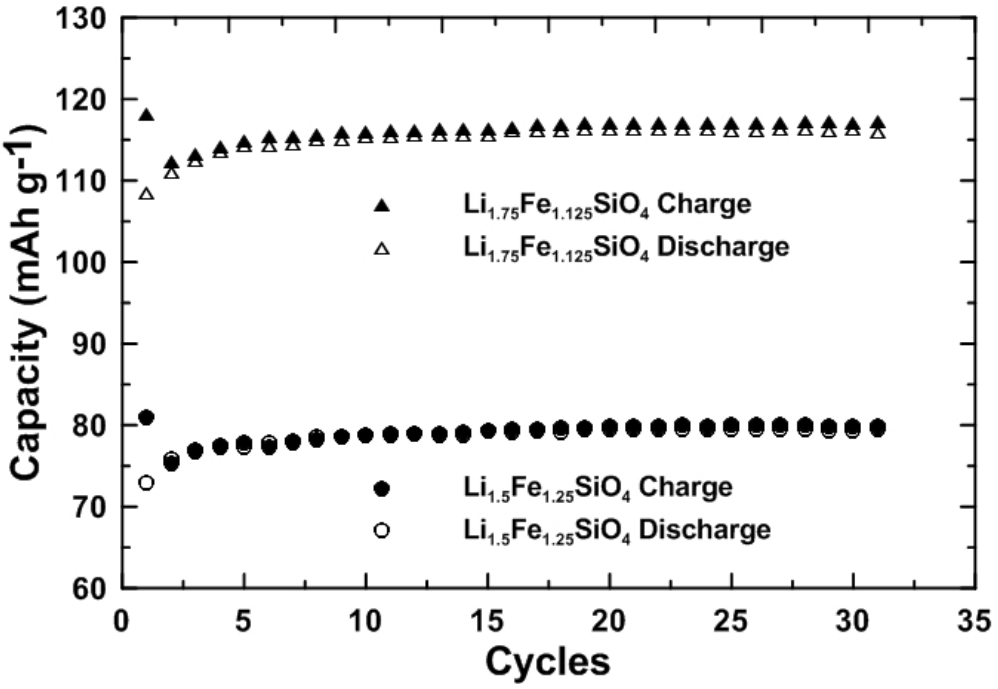

Figure 4.11: *Cycling data for carbon coated $Li_{1.75}Fe_{1.125}SiO_4$ and $Li_{1.5}Fe_{1.25}SiO_4$*

4.4 Conclusion

In this chapter, we have demonstrated that it is possible to synthesize Li_2FeSiO_4 from low cost precursors via a simple solid-state method. The synthesis gave rise to a pure material with large particle size that formed large agglomerates. The material was milled to reduce particle size and carbon coated in order to obtain good electrochemical data. Unfortunately, theoretical capacity was not reached for these samples. The most probable reason behind the mediocre electrochemical performance was that even after milling the particle size was still quite large. An attempt was made to modify the stoichiometry of the material in order to accommodate more iron and less lithium in the crystalline lattice. For $Li_{1.75}Fe_{1.125}SiO_4$, no impurities were detected suggesting the possibility of a pure phase although this would have to be confirmed in a more detailed structural investigation. In the case of $Li_{1.5}Fe_{1.25}SiO_4$ an impurity was noticed from the XRD data suggesting the presence of Fe_2SiO_4. Unfortunately, the two samples did not show improved electrochemical performance over Li_2FeSiO_4.

4.5 References

1. Nyten, A.; Aboumrane, A.; Armand, M.; Gustafson, T.; Thomas, *J. O. Electrochem. Commun.* **2005**, 7, 156.
2. Deng, G.; Zhang, S.; Fu, B. L.; Yang, S.Y.; Ma, L., *Mat. Chem. and Phys.*, **2009**, 120, 14.
3. Fan, X.-Y.; Li, Y.; Wang, J.-J.; Gou, L.; Zhao, P.; Li, D.-L.; Huang, L.; Sun, S.-G., *J. Alloys Compd*, **2010**, 493, 77.
4. Zaghib, K.; Ait Salah, A.; Ravet, N.; Mauger, A.; Gendron, F.; Julien, C. M., *J. Power Sources*, **2006**, 160, 1381.
5. Boulinea, A.; Sirisopanaporn, C.; Dominko, R.; Armstrong, A., R.; Bruce, P., G.; Masquelier, C., *Dalton Trans*., **2010**, 39, 6310
6. Galoustov, K.; Anthonisen, M.; Ryan, D. H.; MacNeil, D. D., *J. Power Sources*, **2011**, 196, 6893
7. Kang, B.; Ceder, G., *Nature*, **2009**, 458, 190
8. Dreyer, W.; Jamnik, J.; Guhlke, C.; Huth, R.; Moskon, J.; Gaberscek, M., *Nature*, **2010**, 9, 448
9. Daheron, B.; MacNeil, D. D., *J. Solid State Electrochem*., Article in press

Chapter 5

Conclusion and Perspectives

5.1 Conclusion

In this thesis, two different cathode materials were investigated. The first material was $LiFePO_4$, where the study consisted of characterizing the mechanism of two different lithiation procedures using an amorphous $FePO_4$ precursor. At each step during the reaction, the products were fully characterized. The result of this investigation was published in the Journal of Power Sources [1]. The second study was on Li_2FeSiO_4, where a novel synthesis was developed using low cost precursors and basic laboratory equipment to minimize the synthetic cost. In addition, an attempt was made to produce off-stoichiometric Li_2FeSiO_4 compounds to increase the electrochemical capacity of the material.

In Chapter 3 of this thesis, two different reactions that produce $LiFePO_4$ starting with amorphous $FePO_4$ were evaluated. The first reaction involved precipitating amorphous $FePO_4$ from a solution of $FeSO_4.7H_2O$ and $NH_4H_2PO_4$ by adding H_2O_2. The lithiation reaction was performed in IPA using lithium acetate and ascorbic acid [2]. The second method involved precipitating hydrated amorphous $FePO_4$ from an solution of $Fe(SO_4)_4(NH_4)_4.6H_2O$ and $NH_4H_2PO_4$ with H_2O_2. The lithiation step was performed using lithium iodide in acetonitrile [3]. The dehydrated $FePO_4$ in both reactions was obtained by thermally treating the precipitated $FePO_4$ at 400 °C for 24 hours. The product of the lithiation reactions was then thermally treated

to produce crystalline $LiFePO_4$. Authors using similar reaction schemes in the literature have suggested that the lithiated product is amorphous $LiFePO_4$ and that only a phase change from amorphous to crystalline $LiFePO_4$ occurs during thermal treatment [2, 3]. Initially, it was of our interest to understand the electrochemical properties of this amorphous $LiFePO_4$ phase, since it has never been studied previously in the literature. Therefore, the literature reactions were reproduced and each step was characterized by X-ray diffraction and Mössbauer Spectroscopy. The data from Xray diffraction was in agreement with what was obtained previously in the literature. From the Mössbauer Spectroscopy data it was concluded that the lithiated product obtained from both lithiation methods contained a large amount of iron in the 3+ oxidation state when starting from either hydrated or dehydrated $FePO_4$. This implied that the lithiation reaction (reduction) did not go to completion. After thermal treatment of the lithiated product an almost pure Fe^{2+} species is obtained. Since a large amount of Fe^{3+} was present before the thermal treatment and almost pure Fe^{2+} species is obtained after, it was concluded that the thermal treatment is essential for the formation and reduction of $LiFePO_4$. It was also noted that when starting with dehydrated $FePO_4$ the samples could be lithiated to a greater extent. In this study it was emphasized that it is essential to use Mössbauer Spectroscopy when dealing with amorphous compounds [1].

In Chapter 4 of this thesis, a novel synthesis for Li_2FeSiO_4 was developed. The goal of this work was to develop a cost effective method to produce Li_2FeSiO_4 by using low cost precursors and standard laboratory equipment. The precursors (Li_2CO_3, SiO_2, Fe_2O_3 and ß-lactose) were mixed by ball milling followed by a thermal treatment. The temperature of the synthesis and the starting ß-lactose content were optimized to produce pure Li_2FeSiO_4. The

sample was milled, carbon coated and electrochemically tested. Carbon coated Li_2FeSiO_4 gave rise to electrochemical capacity of 120 mAh $g^{-1,}$ equivalent to 73% of its theoretical capacity (166 mAh g^{-1} for 1 electron reaction) and no capacity loss was observed over 31 cycles.

An attempt was also made to synthesize off-stoichiometric samples of $Li_{2-2x}Fe_{1+x}SiO_4$ with x = 0.125 and 0.25. The goal was to decrease the amount of lithium and increase the amount of iron in the structure in order to possibly extract more lithium from the oxidation of Fe^{2+} to Fe^{3+}. The method of synthesis for the off-stoichiometric samples was the same as for Li_2FeSiO_4. Carbon coated samples, $Li_{1.75}Fe_{1.125}SiO_4$ and $Li_{1.5}Fe_{1.25}SiO_4$, gave rise to 117 and 79 mAh g^{-1} respectively. For both samples, the capacity values were stable during 31 cycles.

5.2 Perspectives

As mentioned in Chapter 3, the second lithiation reaction which involved dehydrated amorphous $FePO_4$ with LiI in acetonitrile produced one sample that contained 56% of Fe^{2+} species before thermal treatment. Adjusting the conditions in order to push the reduction of iron to completion would be an interesting direction to pursue. If successful it would result in an amorphous sample that contains iron in only the +2 oxidation state. It would also be interesting to understand the coordination of Fe^{2+} in the post lithiated samples. In Chapter 3, no analysis of the structure of iron in the lithiated samples was performed. From the obtained data, the authors could not conclude whether the Fe^{2+} in the lithiated sample was of olivine nature or not. A more detailed structure characterization, by techniques such as Mössbauer spectroscopy, would help elucidate the structure around the iron atoms.

Also, it would be interesting to observe the electrochemical data of the partially lithiated sample as well as the fully lithiated sample. Such electrochemical data would be interesting since to our knowledge, no electrochemical data of amorphous $LiFePO_4$ has been published. Amorphous $LiFePO_4$ may give rise to good electrochemical performance, particularly at high rates, since it was suggested previously that lithium ion can migrate quickly in amorphous structures [4].

Another path for further research would be optimizing the synthesis of Li_2FeSiO_4 such that higher electrochemical performance could be obtained. This could be achieved by improving the milling methods to produce nano-sized material. By using precursors of smaller particle size and shorter heating time, the final particle size of the material could be improved and one may avoid the formation of large agglomerates. As mentioned previously in Chapter 2, large particle size material is not desired since the lithium ion has to migrate from the inside of the particle to the surface. The larger the particle, the longer will be the diffusion path and the diffusion time. Therefore, at higher current rates the lithium that is contained within the center of the particle will not be extracted as rapidly as surface ions, which will ultimately result in poor electrochemical performance. A battery manufactured from large particle size materials could possibly only operate at very low current rates, thereby reducing it practicality. By reducing the particle size and increasing the surface area of the active materials, the diffusion path will be reduced and the lithium ion would have to travel shorter distances in order to access the electrolyte faster. This should lead to better electrochemical performance and possibly better rate capabilities.

Also, another possibility for future work would be to synthesize substituted samples of $Li_{2-2x}Fe_{1+x}SiO_4$ with x = 0.01 up to 0.1 with increments of 0.01. This would be interesting to pursue along with detailed structural analysis of each sample. In addition, electrochemical performance of such samples may lead to higher capacity compared to Li_2FeSiO_4 due to a larger amount of iron in the structure. The iron coordination and oxidation state could be analyzed by Mössbauer Spectroscopy. It has been previously suggested that Li_2MnSiO_4 has three dimensional lithium diffusion [5]. Assuming that Li_2FeSiO_4 is structurally equivalent to Li_2MnSiO_4, that would suggest that the lithium atoms in Li_2FeSiO_4 also migrate via different paths in all three dimensions. Therefore by replacing some of the atoms of lithium by additional iron atoms, the lithium diffusion paths should not be blocked. By synthesizing different samples with small increments of x, one could analyze the structure of the material to understand where exactly the iron atom sits in the lattice and how much substitution can the structure hold until forming an undesired impurity. In the case of $LiFePO_4$, increased conductivity was observed previously in the literature by substituting transition metal atoms in the lithium site at concentrations typically around 1% [6]. Analogously, by substituting small amounts of iron in the lithium site, within the silicate, one can possibly observe improvement in conductivity of the material.

5.3 References

1. Galoustov, K.; Anthonisen, M.; Ryan, D. H.; MacNeil, D. D., *J. Power Sources*, **2011**, 196, 6893
2. Wang, B.; Qiu, Y.; Ni, S., *Solid State Ionics*, **2007**,178, 843.
3. Prosini, P. P.; Carewska, M.; Scaccia, S.; Wisniewski, P.; Passerini, S.; Pasquali, M., *J. Electrochem. Soc.*, **2002**, 149, 886.
4. Kang, B.; Ceder, G., *Nature*, **2009**, 458, 190.
5. Kuganathan, N.; Islam, M., S. *Chem. Mater*. **2009**, 21, 5196.
6. Chung, S.-Y.; Bloking, J., T.; Chiang, Y.-M., *Nature Materials* **2002**, 2, 123.